

POLYMER BRUSHES: PROMISING PLATFORMS FOR CELL FOULING RESISTANCE,  
CELL SORTING, AND TARGETED DRUG DELIVERY

by

AMINE M LARADJI

(Under the Direction of Sergiy Minko)

ABSTRACT

The aim of this work is to synthesize surface-tethered polymer chains with different functionalities and properties to address some of the challenging questions the biomedical field currently faces. In particular, we have successfully synthesized densely grafted polymer brush-coated silicon wafers by the grafting to approach and investigating their antifouling properties. Next, the design and synthesis of a patterned responsive mixed polymer brush platform for bond control between cells and the peptide RGD is discussed. The latter platform was applied to detect rare cancer cells from mouse blood and demonstrated efficient isolation and high recovery of target cells. Finally, we have developed a stimuli responsive platform useful for targeted drug delivery that can be remotely controlled with a magnetic field. Intermediate and final products in the research projects here mentioned have been investigated using atomic force microscopy, ellipsometry, fluorescence spectroscopy, dynamic light scattering, nuclear magnetic resonance, FTIR and mass spectrometry.

INDEX WORDS: polymer brushes, click chemistry, grafting to, grafting from, antifouling, drug delivery, cell adhesion, integrin, RGD, cancer cells, magnetic nanoparticles

POLYMER BRUSHES: PROMISING PLATFORMS FOR CELL FOULING RESISTANCE,  
CELL SORTING, AND TARGETED DRUG DELIVERY

by

AMINE M LARADJI

B.S, Ecole Nationale Polytechnique, Algeria, 2000

M.S, Tennessee State University, 2013

A Dissertation Submitted to the Graduate Faculty of The University of Georgia in Partial

Fulfillment of the Requirements for the Degree

DOCTOR OF PHILOSOPHY

ATHENS, GEORGIA

2018

© 2018

AMINE M LARADJI

All Rights Reserved

POLYMER BRUSHES: PROMISING PLATFORMS FOR CELL FOULING RESISTANCE,  
CELL SORTING, AND TARGETED DRUG DELIVERY

by

AMINE M LARADJI

Major Professor:	Sergiy Minko
Committee:	Vladimir Popik
	Robert Phillips

Electronic Version Approved:

Suzanne Barbour  
Dean of the Graduate School  
The University of Georgia  
May 2018

## ACKNOWLEDGEMENTS

First and foremost, I would like to express my sincere appreciation and gratitude to my advisor Professor Sergiy Minko for his continuous support, constructive advice, and insightful guidance that were stimulating and motivational throughout my research under his supervision. I would also like to acknowledge the members of my committee: Dr. Popik and Dr. Phillips for providing valuable suggestions and ideas in addition to their support. Finally, I would like to thank all faculty and staff members of the department of chemistry and department of textiles, merchandising, and interior.

## TABLE OF CONTENTS

	Page
ACKNOWLEDGEMENTS .....	iv
LIST OF TABLES .....	vii
LIST OF FIGURES .....	viii
CHAPTER	
1. INTRODUCTION AND LITERATURE REVIEW .....	1
1.1. Polymer Brush Synthesis. ....	2
1.2. Polymer Brush Characterization. ....	3
1.3. Stimuli-Responsive Polymer Brushes.....	5
1.4. Mixed Polymer Brushes.....	7
1.5. Polymer Brushes for Proteins Biofouling.....	8
1.6. Polymer Brushes for Cell Adhesion Regulation.....	9
1.7. Polymer Brushes for Drug Delivery. ....	11
1.8. Research Objectives.....	12
1.9. References.....	14
2. ROBUST, SOLVENT-FREE, CATALYST-FREE CLICK CHEMISTRY FOR THE GENERATION OF HIGHLY STABLE DENSELY GRAFTED POLY(ETHYLENE GLYCOL) POLYMER BRUSHES BY THE GRAFTING TO METHOD AND THEIR PROPERTIES .....	22
2.1. Introduction.....	23

2.2. Experimental Section.....	26
2.3. Results and Discussion.....	28
2.4. Conclusion.....	37
2.5. References.....	37
3. A STIMULI-RESPONSIVE SWITCHABLE INTERFACE FOR MAMMALIAN CELLS	
STIMULATION AND CANCER CELLS DETECTION.....	42
3.1. Introduction.....	43
3.2. Experimental Section.....	45
3.3. Results and Discussion.....	49
3.4. Conclusion.....	59
3.5. References.....	60
4. MAGNETICALLY CONTROLLED DRUG DELIVERY SYSTEM FOR IMPLANT	
INFLAMMATION.....	65
4.1 Introduction.....	66
4.2 Experimental Section.....	69
4.3 Results and Discussion.....	73
4.4 Conclusion.....	79
4.5 References.....	79
5. SUMMARY AND FUTURE OUTLOOK.....	
5.1 Summary.....	86
5.2 Future Work.....	86

## LIST OF TABLES

	Page
Table 2.1. Characteristics of PEG brushes .....	32
Table 3.1. PAA and PAA-RGD thicknesses (in nm) in air and liquid .....	52

## LIST OF FIGURES

	Page
Figure 1.1. Schematic illustration of polymer brush synthesis via the grafting to and the grafting from.....	3
Figure 1.2. Behavioral schematic illustration of thermo and pH responsive polymers.....	5
Figure 1.3. Schematic illustration of morphological changes upon exposure with nonselective solvent (A), and selective solvents (B, C).....	8
Figure 1.4. Schematic illustration of protein repellency upon surface coating.....	8
Figure 1.5. Chemical structure of poly(ethylene glycol).....	9
Figure 1.6. In-vitro cell adhesion stages.....	10
Figure 1.7. Comparison of cell harvesting methods.....	11
Figure 1.8. Magnetic nanoparticles loaded with an enzyme (E-particle) and substrate-drug conjugate (S-particles). Cryo-transmission electron microscopy (a), Schematic illustration of the drug release working concept.....	12
Figure 2.1. Preparation of PEG brushes via solvent-free, catalyst-free click reaction.....	26
Figure 2.2. PGMA thickness increase upon photo-DIBO immobilization.....	30
Figure 2.3. PEG films (from 5 Kg/mol) thickness (a) and grafting density (b).....	31
Figure 2.4. Effects of time and PEG Mn on films thickness (a, c) and grafting densities (b, d)...	33
Figure 2.5. Step-by-step ellipsometric thickness maps of polymer brushes prepared from 5, 10, and 20 Kg/mol Mn of PEG on Si-wafers demonstrating the layers of silica (a), PGMA-DIBO (b) and PEG brushes (a-c).....	34

Figure 2.6. Fluorescence microcopy images of PEG brushes (from 5, 10, and 20 Kg/mol) after their incubation in a solution of BSA-FITC in PBS .....	35
Figure 2.7. Fluorescence microscopy images of PEG films (5 Kg/mol) after incubation in PBS buffer for various periods.....	36
Figure 3.1. Fitted curve of NIPAM arget ATRP kinetics from substrate-coated initiators .....	49
Figure 3.2. AFM morphology and thickness profile of the PNIPAM brush (80 nm) in dry .....	50
Figure 3.3. Ellipsometric $\Delta$ (a), $\psi$ (b) changes and thickness (c) changes with temperature.....	51
Figure 3.4. AFM images and height profile of PNIPAM thickness characterizing thickness change with temperature above (a, b) and below (c,d) the LCST .....	51
Figure 3.5. AFM of PNIPAM-PAA brushes in dry (a), collapsed (b) and swollen state (c).....	53
Figure 3.6. 3T3 cells attached to PNIPAM thickness (nm) of 0 (a), 18 (b), 80 (c), and 150 (d)...	54
Figure 3.7. Cells release From PNIPAM thickness (nm) of: 0 (a), 18 (b), 80 (c), and 150 (d).....	55
Figure 3.8. Adhesion and detachment of U87 cells (a) and blood cells (b).....	57
Figure 3.9. U-87MG cells separation by temperature oscillation (a-e) and continuous (f) .....	58
Figure 3.10. U-87 MG cells recovery after final temperature oscillation.....	59
Figure 4.1. Illustration of the working concept of the stimuli responsive model implant.....	69
Figure 4.2. FTIR grazing angle (a) and ellipsometry maps (b) of the substrate layers .....	74
Figure 4.3. AFM height images of Si-BIBB(a), Si-PGMA(b), Si-BSA(c), and Si-POEGMA(d).	75
Figure 4.4. FTIR spectra(a), enzyme activity of MNPs-TRY(b), and particle size by DLS of MNPs(black), MNPs-Si(purple), MNPs-PGMA(green), and MNPs-POEGMA(red)(c) ..	77
Figure 4.5. Thickness of POEGMA effects on proteolysis .....	78
Figure 4.6. BSA-FitC proteolysis under and without the influence of a magnetic field .....	79

## 1. INTRODUCTION AND LITERATURE REVIEW

Polymer brushes are tethered polymer chains by one end to a substrate where the polymer coils are forced to stretch away from the surface in order to avoid overlapping.<sup>1</sup> For the brush regime to exist, the following conditions are to be met: the brush height is greater and the distance between grafting point is less than two times of the radius of gyration of the polymer chain or  $h > 2(R_g^2)^{1/2}$ ,  $d < 2(R_g^2)^{1/2}$ , where  $d$  is the distance between the grafting points,  $h$  is the brush height in a given solvent, and  $(R_g^2)^{1/2}$  is the radius of gyration of the same non grafted chain dissolved in the same solvent.<sup>2</sup>

Theoretically, the firsts polymer brush descriptions were provided by Alexander<sup>3</sup> and de Gennes.<sup>4</sup> Upon increased grafting density, one polymer chain can be assimilated as blobs where a number of monomers are confined into each blob. When the grafting density increases even more, the number of monomers in every blob decreases significantly to avoid excluded volume effects and as a result of that the polymer chains stretch normally to the surface. These descriptions have been later followed by theories arguing about the uniformity of the image provided by the former descriptions by claiming that the polymer chains end might be found anywhere within the brush and not necessary at the end of the brush.<sup>5</sup>

For nearly 50 years, polymers at interfaces have drawn an immense attention from physicists and chemists alike due to their effects on coated surfaces and their potential applications in various fields. The first interesting observation reported was in the 1950s when it was observed that colloidal particles coagulation could be thwarted upon coating them with polymer chains.<sup>6-8</sup> Now and after decades of theoretical and experimental studies on tethered polymer chains, more

applications are currently either implemented in real life situations or are under investigations for potential use at an industrial scale.

### **1.1. Polymer Brush Synthesis**

Polymer brushes can be generated either through covalent bonding, or physical bonding such as electrostatic interactions, hydrogen bonding, or Van Der Waals interaction. However, since physical grafting is weak, this approach is less durable and may result in bond destruction and/or deformation of soft substrates.<sup>2</sup> Grafting polymer chains covalently to create polymer brushes can be synthesized via two major approaches, namely the “grafting from” approach which relies on in situ polymerization from an initiator pre-immobilized on a substrate, and the “grafting to” approach when polymer chains are tethered to the surface via a chemical reaction between complementary functional groups of the polymer chains and the surface.<sup>9</sup> Both grafting to and grafting from methods have advantages and disadvantages. For example, while the grafting from technique can achieve higher grafting thicknesses and consequently, higher grafting densities (chains/nm<sup>2</sup>), polymers grafted with this approach cannot be characterized for their molecular weights and polydispersity, and are less stable in aqueous media as a result of silanes hydrolysis in water.<sup>10</sup> On the other hand, while the grafting to approach is rather simple and grafted polymers can fully be characterized, it lacks high grafting densities due to steric hindrances that increase with increasing brush thickness.<sup>11</sup> To yield polymer brushes by the grafting to approach, a number of chemical reactions have been used and investigated for their effects on the grafting density or on their intended application.<sup>12-15</sup> Among all these reactions used, click reactions remain the most attractive due to their simplicity, high yielding, and orthogonality.<sup>16</sup> For example, copper(I)-catalyzed Huisgen 1,3-dipolar cycloaddition has been previously reported for polyethylene glycol grafting on silicon wafers.<sup>15</sup> However, limited grafting densities were

obtained. Furthermore, the copper catalyst used in this reaction is toxic, which limits the usefulness of polymer brushes for medical and biological applications.

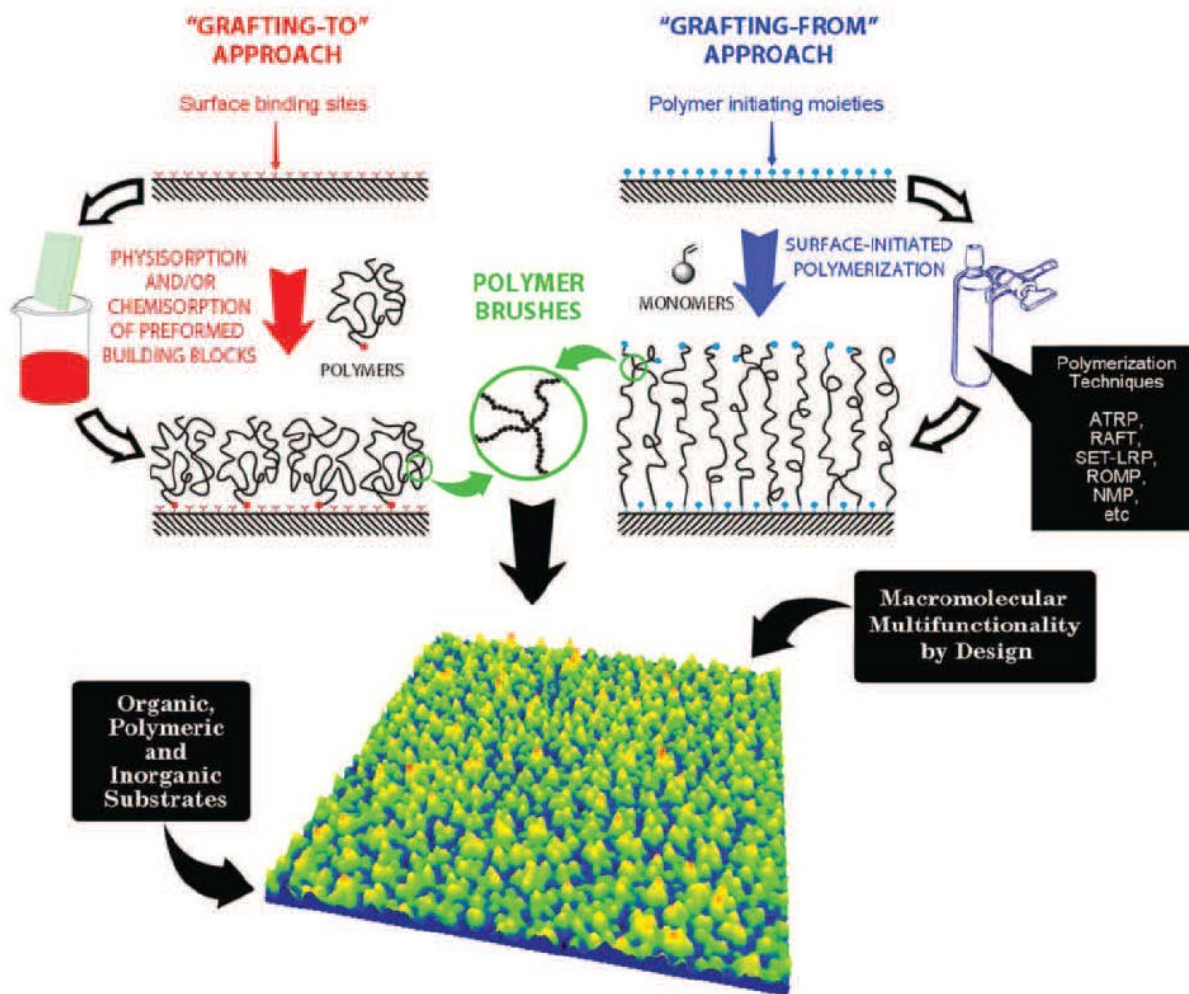


Figure 1.1. Schematic illustration of polymer brush synthesis via the grafting to and the grafting from.<sup>17</sup> Adapted with permission of publisher.

## 1.2. Polymer Brush Characterization

In order to characterize polymer brushes, different techniques are nowadays available, and each available technique is suitable for a particular property. For example, the existence of certain functional groups within a thin film can be probed by IR spectroscopy, and grazing-angle reflection-absorption IR spectroscopy when the films are too thin to be detected by normal IR

spectroscopy.<sup>18</sup> XPS is another powerful tool that can convey qualitative as well as quantitative information about polymer coatings.<sup>9</sup> Limited to conducting samples, Auger electron spectroscopy (AES) has also been used to determine polymer brushes chemical composition.<sup>19</sup>

The most characterized property of polymer brushes is their thicknesses. This is often done using ellipsometry due to its accuracy and convenience.<sup>9</sup> However, Atomic Force Microscopy (AFM) is also commonly used for the same purpose. For polymer brushes grown from nanoparticles, transmission electron microscopy (TEM)<sup>20</sup> and dynamic light scattering (DLS)<sup>21</sup> are a routinely used techniques to determine brush thicknesses. Surface structure of polymer brushes and their topography can be characterized by the following: AFM,<sup>22</sup> scanning electron microscopy (SEM)<sup>23</sup> fluorescence microscopy<sup>24</sup> or XPS mapping.<sup>25</sup> Finally, the polymer chains molecular weight might be investigated using gel permeation chromatography (GPC). However, this property is quite challenging to characterize since polymer chains are tethered to a surface. For that reason, cleavage of tethered polymer chains has been attempted mainly from nanoparticles to provide detectable amounts of polymer chains. There are currently two possible ways that are used to achieve the cleavage of polymer chains from surfaces; the first one is by using strong acids such as hydrofluoric acid<sup>26</sup>, however this approach has safety concerns and undesired side effects, while the second approach relies on adding linkers between the polymer chains and the surface. The latter approach though attractive; it requires complex and time consuming synthesis to prepare the special linkers.<sup>27</sup> The most frequently used method to determine the molecular weight of polymer brushes is, however, based on adding a sacrificial initiator during the polymerization reaction assuming that the polymerization rate from the surface and in solution are similar. This assumption has however has been shown in number of times that is not always true.<sup>27</sup> One reason for the observed discrepancy is the heterogeneous nature of surface-initiated

polymerizations where, unlike in solution, the reactants and catalysts diffusion to the surface is a limiting factor.

### 1.3. Stimuli-Responsive Polymer Brushes

Stimuli responsive polymer brushes (SRPB) are a special class of polymer brushes that are capable of undergoing conformational changes when subjected to external stimuli. Examples of stimuli include: temperature,<sup>28-29</sup> light,<sup>30-31</sup> and pH.<sup>32-33</sup> Temperature-sensitive polymers are termed thermoresponsive polymers because, under temperature effects, they undergo a reversible phase change that results in stretch-collapse transition of the polymer brush.<sup>34</sup> Thermoresponsive polymers with a lower critical solution temperature (LCST) collapse when heated above their LCST, while those with an upper critical solution temperature (UCST) collapse when cooled under their UCST (figure 1.2).<sup>34</sup>

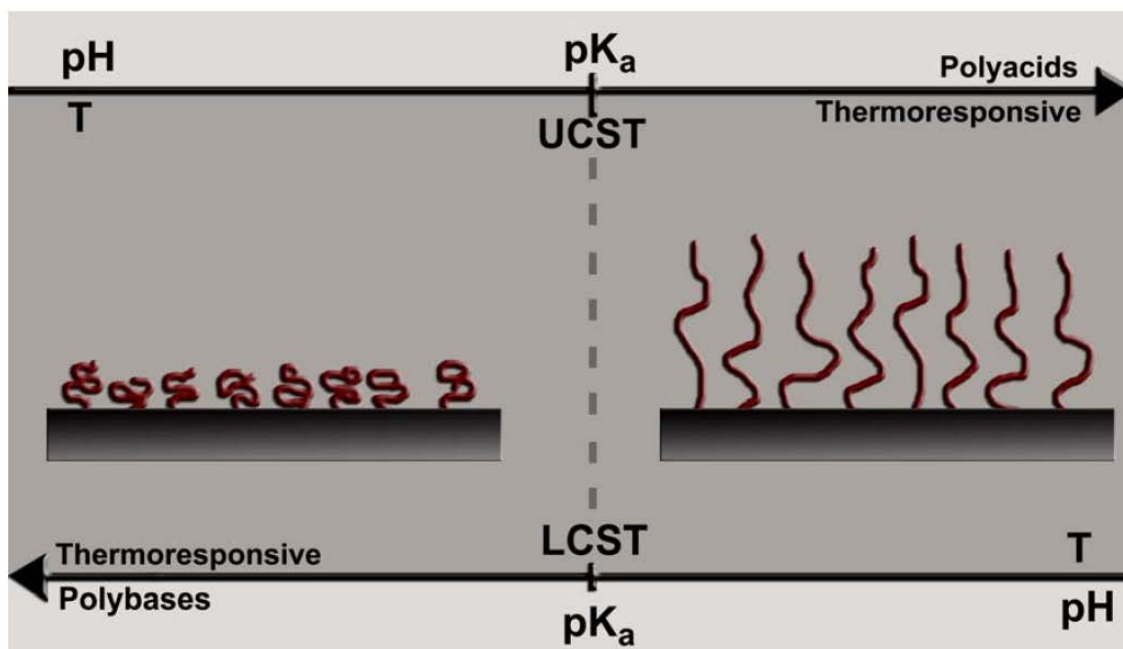


Figure 1.2. Behavioral schematic illustration of thermo and pH responsive polymers.<sup>34</sup> Adapted with permission of publisher.

As a result of such reactions, stimuli-responsive polymers have been suggested for numerous applications in every possible field mainly in the biomedical field where a considerable number of reviews are currently available.<sup>35-37</sup>

In the drug delivery area, stimuli-responsive polymers have long been desired due to their potential benefits over traditional approaches in delivering drugs that includes higher bioavailability at the target sites relative to others, decreased undesired drugs sides effects, and improved patient's compliance. These systems are based on loading a drug of interest into a polymeric material followed by its release, once administered, into a specific target using either an external or internal stimuli to trigger the release. The polymeric carrier has to be non-toxic, biocompatible, and biodegradable.<sup>38</sup> Drug delivery systems have been designed to deliver therapeutics when stimulated by near-infrared light,<sup>39-41</sup> pH changes,<sup>42-43</sup> externally applied magnetic field,<sup>44</sup> and enzymes.<sup>45-46</sup> In particular, the later trigger is especially promising considering the high selectivity of enzymes and their elevated catalytic properties. More importantly, enzymes' overexpression has been associated with certain cells abnormalities, which makes it possible to design smart drug delivery systems to selectively target those specific cells.<sup>47</sup> Nevertheless, targeted drug release based on enzymes' over-expression is limited. In fact, the concentration of enzymes on target cells as well as the concentration difference of enzymes between the target and non target sites may not be high enough to allow specific drug release.<sup>48</sup>

Another application of stimuli responsive materials within the medical and biological fields is in cell culture. For example, poly(N-isopropylacrylamide) (PNIPAm) was grafted on polystyrene surface, and cells were cultured on it at 37 °C.<sup>49</sup> Upon lowering the temperature to below 32 °C cells were observed to detach from the surface. This smart cell culture surface has switching behaviour thanks to the thermoresponsiveness of

PNIPAm. In fact, this polymer undergoes a reversible phase change at LCST of about 32°C from collapsed chains above the LCST to extended chains below its LCST. At 37°C, the surface becomes hydrophobic which leads to protein adsorption and cells adhesion consequently. At room temperature, however, the polymer chains become hydrophilic and switch the adhesion off as a result of that. This capability of stimuli-responsive interfaces is important as it can be utilized in mammalian cell research where the signal-triggered exposure of functional molecules in controlled sequences could be used to stimulate cell responses and mimic conditions for the growth and differentiation of cells in the extracellular matrix. Moreover, it will be possible to decode and interpret biochemical mechanisms, which are important in understanding the biochemistry and biophysics of cells that, ultimately, could help in developing drugs and therapeutics methods.

#### **1.4. Mixed Polymer Brushes**

Mixed polymer brushes are another special class of polymer brushes and are made by the confinement of more than one kind of polymer chains to the surface. These types of polymer brushes are also responsive to their environment by switching their structure between different phase-segregated morphologies.<sup>50-51</sup>

Figure 1.3 illustrates an example of a mixed polymer brush made of one polymer that is hydrophilic while the other is hydrophobic. The surface properties of this thin film can actually be switched from hydrophobic, by swelling the hydrophobic polymer chains in a non polar solvent, to hydrophilic by treating the thin film with a polar solvent to swell the hydrophilic polymer chains.<sup>52</sup>

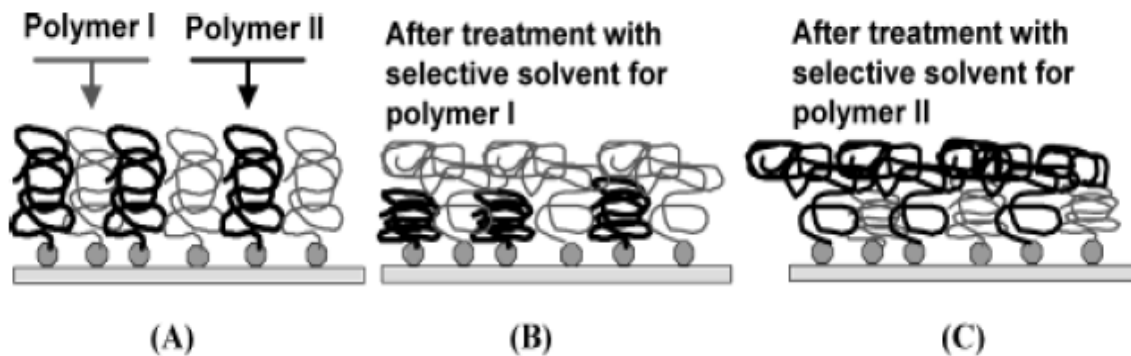


Figure 1.3. Schematic illustration of morphological changes upon exposure with nonselective solvent (A), and selective solvents (B, C).<sup>52</sup> Adapted with permission of publisher.

### 1.5. Polymer Brushes for Proteins Biofouling

Biofouling is the propensity of materials of biological origin, such as proteins, to adsorb physically on surfaces.<sup>53</sup> Some reasons behind the accumulation of proteins on surfaces include: hydrophobic and/or electrostatic interactions. It is of crucial importance for successful application of many new technologies to develop materials that can resist proteins fouling. As an example, implanted medical devices for diagnosis or therapeutics purposes can easily be compromised if colonized by biological materials, which would ultimately lead to devices removal. Up to now, surface passivation remains one of the popular approaches to reduce the nonspecific adsorption of proteins on surfaces (figure 1.4).

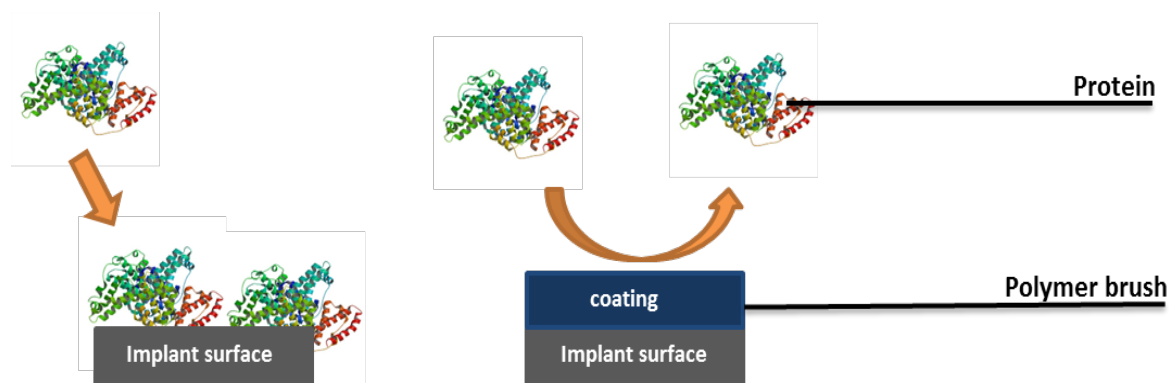


Figure 1.4. Schematic illustration of protein repellency upon surface coating.

This strategy consists of coating surfaces with biocompatible and neutral polymer chains such as poly(hydroxyethyl methacrylate), poly(acrylamide), poly(N,N-dimethyl acrylamide), dextran, and poly(ethylene glycol).<sup>53</sup> The latter mentioned polymer, however, remains the most widely used and investigated polymer for that purpose (Figure 1.5).<sup>54</sup>

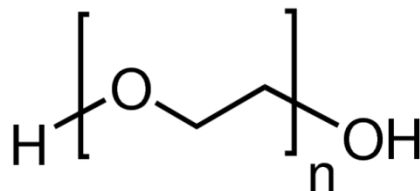


Figure 1.5. Chemical structure of poly(ethylene glycol).

Despite the fact that the protein repellency mechanism of poly(ethylene glycol) is not well understood, a number of reasons have been suggested to account for this behavior. Among them are: hydrophilicity, mobility.<sup>55</sup> Furthermore, protein adsorption is prevented by steric hindrance due to the existence of the ethoxy repeat unit that can form a hydration layer through hydrogen bonds.<sup>54</sup> Besides the chemical composition of the polymer, the effectiveness of poly(ethylene glycol)-based coatings also depend on their physical properties such layer thickness, grafting density, and uniformity, with higher films thickness resulting in lower protein adsorption.<sup>56</sup> However, poly(ethylene glycol) is prone to oxidative degradation in aqueous media,<sup>57-58</sup> and, therefore, other alternatives to poly(ethylene glycol)-coated surfaces have been investigated for their antifouling properties, such as zwitterionic polymers,<sup>59</sup> amino acid-based zwitterionic polymers,<sup>60</sup> and zwitterionic polysaccharides.<sup>61</sup>

## 1.6. Polymer Brushes for Cell Adhesion Regulation

Cell adhesion regulation is another application where polymer brushes have been used. Cell adhesion is defined as the capability of cells to adhere to other cells or to the extracellular matrix

(ECM).<sup>62</sup> This behavior is central to cells communication and tissues maintenance and development.<sup>63</sup>

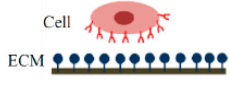
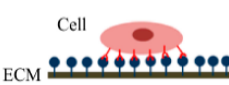
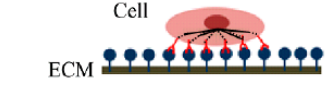
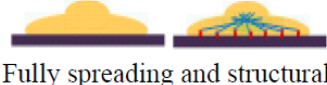
Cell Adhesion Phases	Phase I	Phase II	Phase III
Schematic diagram of cell adhesion			
Schematic diagram of the transformation of cell shape			
Cell adhesion intervention	Electrostatic interaction	Integrin bonding	Focal adhesion
Adhesion stages	Sedimentation	Cell attachment	Cell spreading and stable adhesion

Figure 1.6. In-vitro cell adhesion stages.<sup>62</sup> Adapted with permission of publisher.

Figure 1.6 illustrates the main stages of cell adhesion where the mechanism consists first by initial attachment of the cell to the host surface through physical interactions, followed by bonding of the cell to the surface through cell integrin. This stage is characterized by the flattening of the cell body. And finally, the cell spreads to reach a maximum area through increased adhesion strength.<sup>62</sup>

To regulate cells adhesion, temperature-sensitive polymer chains are more commonly used materials for that purpose. For example, poly(N-isopropyl acrylamide) were grafted on glass substrates and used to tune the adhesiveness of bovine carotid artery endothelial cells (BAECs).<sup>64-65</sup> Poly(N-isopropyl acrylamide) hydrophobicity is used for inducing cells adhesion above 32 °C, while cells detachment occurs at below 32 °C when the polymer becomes hydrophilic. The major advantage of this mechanism concerning cell detachment is the possibility to preserve the cell intact by avoiding common enzyme-induced detachment that results in cell damage.<sup>66</sup>

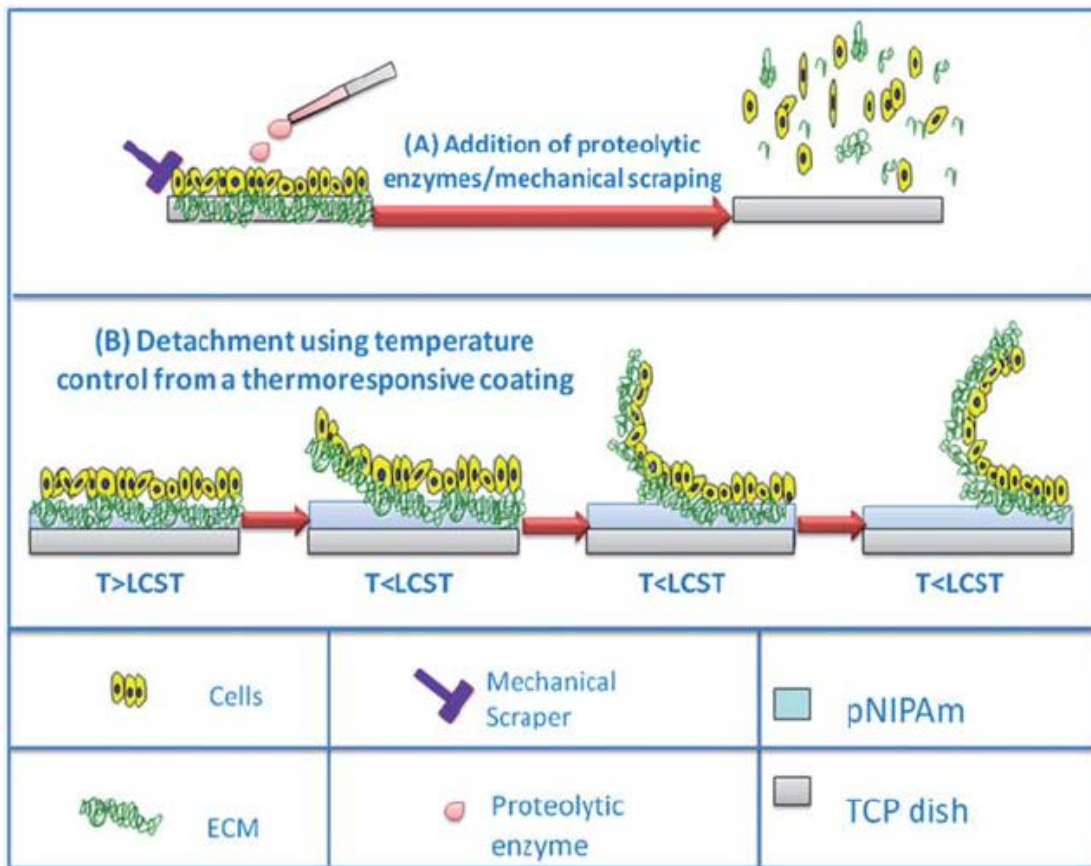


Figure 1.7. Comparison of cell harvesting methods. Adapted from<sup>66</sup> with permission of the Royal Society of Chemistry.

### 1.7. Polymer Brushes for Drug Delivery

In order to increase drug selectivity and decrease its side effects, a number of polymer brush-based materials have been investigated. For their properties, polymer brushes have been introduced to improve nanoparticles dispersion and control their aggregation.<sup>17</sup> A more specific example is the synthesis of copolymer-decorated magnetic nanoparticles where in one part a substrate-drug conjugate is embedded within the polymer chains and the other part contains the substrate-specific enzyme.<sup>67</sup> In that example polymer brushes exerted repulsive interactions between both parts of the nanoparticles to avoid unwarranted drug release via substrate-enzyme reaction (figure 1.8). When an external magnetic field is applied, however, both particles

overcome these steric hindrances and merge together to initiate the drug release through substrate proteolysis.

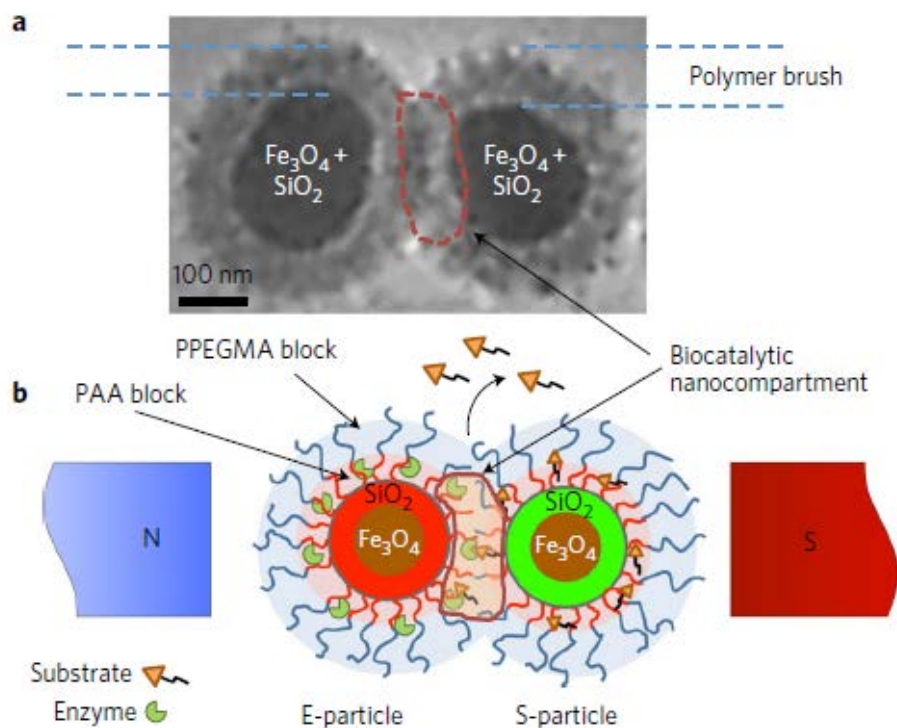


Figure 1.8. Magnetic nanoparticles loaded with an enzyme (E-particle) and substrate-drug conjugate (S-particles). Cryo-transmission electron microscopy (a), Schematic illustration of the drug release working concept. Adapted from<sup>67</sup> with permission.

## 1.8. Research Objectives

### **Paper 1. Robust, Solvent-Free, Catalyst-Free Click Chemistry for the Generation of Highly Stable Densely Grafted Poly(ethylene glycol) Polymer Brushes by the Grafting To Method and Their Properties**

In the second chapter, the development of a novel approach to synthesize densely grafted polymer brushes will be discussed. The primary goals of this research study are:

1. Synthesizing densely grafted polymer brushes by the grafting to approach using a catalyst-free and solvent-free approach.

2. Studying the antifouling properties of the synthesized polymer brush.
3. And studying the long term stability of the polymer brush in aqueous media.

### **Paper 2. A Stimuli-Responsive Switchable Interface for the Stimulation of Mammalian Cells and Cancer Cells Isolation**

In the fourth third, the design and synthesis of a patterned stimuli responsive polymer brush is reported. The designed biointerface was used to switch on and off mammalian cells adhesion simply by changing the temperature of the cell medium. Furthermore, this biomaterial was able to isolate cancer cells from mouse blood at a negligible amount.

Some objectives of this research project are:

1. Syntheses of a thermoresponsive interface and study of its thermal responsiveness.
2. Investigating mammalian cells adhesion and detachment from the biointerface when under the influence of the medium temperature.
3. Cancer cells separation from a complex mixture of blood cells as a complementary method for cancer early detection.

### **Paper 3. Magnetically Controlled Drug Delivery system for Implantable devices**

In the fourth chapter, the development of a novel concept of dual-stimuli responsive platform useful for applications in targeted drug delivery is demonstrated. The platform here synthesized has mainly been applied to deliver a model drug.

The main objectives of the present research are:

1. Synthesis a novel drug delivery platform
2. Proof of concept of the synthesized drug delivery implantable device

## 1.9. References

1. Zhao, B.; Brittain, W. J., Polymer brushes: surface-immobilized macromolecules. *Progress in Polymer Science* **2000**, *25* (5), 677-710.
2. Minko, S., Responsive Polymer Brushes. *Journal of Macromolecular Science, Part C: Polymer Reviews* **2006**, *46* (4), 397-420.
3. Alexander, S., Adsorption of Chain Molecules with a Polar Head a-Scaling Description. *Journal De Physique* **1977**, *38* (8), 983-987.
4. de Gennes, P. G., Conformations of Polymers Attached to an Interface. *Macromolecules* **1980**, *13* (5), 1069-1075.
5. Binder, K., Scaling concepts for polymer brushes and their test with computer simulation. *Eur Phys J E Soft Matter* **2002**, *9* (3), 293-8.
6. Brittain, W. J.; Minko, S., A structural definition of polymer brushes. *J Polym Sci Pol Chem* **2007**, *45* (16), 3505-3512.
7. van der Waarden, M., Stabilization of carbon-black dispersions in hydrocarbons. *Journal of Colloid Science* **1950**, *5* (4), 317-325.
8. van der Waarden, M., Adsorption of aromatic hydrocarbons in nonaromatic media on carbon black. *Journal of Colloid Science* **1951**, *6* (5), 443-449.
9. Barbey, R.; Lavanant, L.; Paripovic, D.; Schuwer, N.; Sugnaux, C.; Tugulu, S.; Klok, H. A., Polymer brushes via surface-initiated controlled radical polymerization: synthesis, characterization, properties, and applications. *Chem Rev* **2009**, *109* (11), 5437-527.
10. Chen, T.; Amin, I.; Jordan, R., Patterned polymer brushes. *Chem Soc Rev* **2012**, *41* (8), 3280-96.

11. Ayres, N., Polymer brushes: Applications in biomaterials and nanotechnology. *Polym. Chem.* **2010**, *1* (6), 769-777.
12. Anne, A.; Demaille, C.; Moiroux, J., Terminal attachment of polyethylene glycol (PEG) chains to a gold electrode surface. Cyclic voltammetry applied to the quantitative characterization of the flexibility of the attached PEG chains and of their penetration by mobile PEG chains. *Macromolecules* **2002**, *35* (14), 5578-5586.
13. Kingshott, P.; McArthur, S.; Thissen, H.; Castner, D. G.; Griesser, H. J., Ultrasensitive probing of the protein resistance of PEG surfaces by secondary ion mass spectrometry. *Biomaterials* **2002**, *23* (24), 4775-85.
14. Sudre, G.; Siband, E.; Hourdet, D.; Creton, C.; Cousin, F.; Tran, Y., Synthesis and Characterization of Poly(acrylic acid) Brushes: "Grafting-Onto" Route. *Macromolecular Chemistry and Physics* **2012**, *213* (3), 293-300.
15. Ostaci, R.-V.; Damiron, D.; Al Akhrass, S.; Grohens, Y.; Drockenmuller, E., Poly(ethylene glycol) brushes grafted to silicon substrates by click chemistry: influence of PEG chain length, concentration in the grafting solution and reaction time. *Polym. Chem.* **2011**, *2* (2), 348-354.
16. Tsai, H. Y.; Vats, K.; the journal ..., Y.-M. Z., Two-Dimensional Micropatterns of Self-Assembled Poly (N-isopropylacrylamide) Microgels for Patterned Adhesion and Temperature-Responsive Detachment .... *Langmuir: the ACS journal ...* **2013**.
17. Azzaroni, O., Polymer brushes here, there, and everywhere: Recent advances in their practical applications and emerging opportunities in multiple research fields. *Journal of Polymer Science Part A: Polymer Chemistry* **2012**, *50* (16), 3225-3258.

18. Yamamoto, S.; Ejaz, M.; Tsujii, Y.; Fukuda, T., Surface interaction forces of well-defined, high-density polymer brushes studied by atomic force microscopy. 2. Effect of graft density. *Macromolecules* **2000**, *33* (15), 5608-5612.
19. Azzaroni, O.; Brown, A. A.; Huck, W. T., UCST wetting transitions of polyelectrolytic brushes driven by self-association. *Angew Chem Int Ed Engl* **2006**, *45* (11), 1770-4.
20. Dey, T., Polymer-coated magnetic nanoparticles: surface modification and end-functionalization. *J Nanosci Nanotechnol* **2006**, *6* (8), 2479-83.
21. Chen, X.; Randall, D. P.; Perruchot, C.; Watts, J. F.; Patten, T. E.; von Werne, T.; Armes, S. P., Synthesis and aqueous solution properties of polyelectrolyte-grafted silica particles prepared by surface-initiated atom transfer radical polymerization. *J Colloid Interface Sci* **2003**, *257* (1), 56-64.
22. Zhou, F.; Zheng, Z.; Yu, B.; Liu, W.; Huck, W. T., Multicomponent polymer brushes. *J Am Chem Soc* **2006**, *128* (50), 16253-8.
23. Ward, J. H.; Bashir, R.; Peppas, N. A., Micropatterning of biomedical polymer surfaces by novel UV polymerization techniques. *J Biomed Mater Res* **2001**, *56* (3), 351-60.
24. Dong, R.; Krishnan, S.; Baird, B. A.; Lindau, M.; Ober, C. K., Patterned biofunctional poly(acrylic acid) brushes on silicon surfaces. *Biomacromolecules* **2007**, *8* (10), 3082-92.
25. Slim, C.; Tran, Y.; Chehimi, M. M.; Garraud, N.; Roger, J. P.; Combellas, C.; Kanoufi, F., Microelectrochemical Patterning of Surfaces with Polymer Brushes. *Chemistry of Materials* **2008**, *20* (21), 6677-6685.
26. Marutani, E.; Yamamoto, S.; Ninjbadgar, T.; Tsujii, Y.; Fukuda, T.; Takano, M., Surface-initiated atom transfer radical polymerization of methyl methacrylate on magnetite nanoparticles. *Polymer* **2004**, *45* (7), 2231-2235.

27. Kang, C. J.; Crockett, R. M.; Spencer, N. D., Molecular-Weight Determination of Polymer Brushes Generated by SI-ATRP on Flat Surfaces. *Macromolecules* **2014**, *47* (1), 269-275.
28. Sun, T.; Wang, G.; Feng, L.; Liu, B.; Ma, Y.; Jiang, L.; Zhu, D., Reversible switching between superhydrophilicity and superhydrophobicity. *Angew Chem Int Ed Engl* **2004**, *43* (3), 357-60.
29. He, Q.; Kueller, A.; Schilp, S.; Leisten, F.; Kolb, H. A.; Grunze, M.; Li, J., Fabrication of controlled thermosensitive polymer nanopatterns with one-pot polymerization through chemical lithography. *Small* **2007**, *3* (11), 1860-5.
30. Fries, K.; Samanta, S.; Orski, S.; Locklin, J., Reversible colorimetric ion sensors based on surface initiated polymerization of photochromic polymers. *Chem Commun (Camb)* **2008**, *0* (47), 6288-90.
31. Samanta, S.; Locklin, J., Formation of photochromic spiropyran polymer brushes via surface-initiated, ring-opening metathesis polymerization: reversible photocontrol of wetting behavior and solvent dependent morphology changes. *Langmuir* **2008**, *24* (17), 9558-65.
32. Sanjuan, S.; Tran, Y., Stimuli-Responsive Interfaces Using Random Polyampholyte Brushes. *Macromolecules* **2008**, *41* (22), 8721-8728.
33. Geoghegan, M.; Ruiz-Pérez, L.; Dang, C. C.; Parnell, A. J.; Martin, S. J.; Howse, J. R.; Jones, R. A. L.; Golestanian, R.; Topham, P. D.; Crook, C. J.; Ryan, A. J.; Sivia, D. S.; Webster, J. R. P.; Menelle, A., The pH-induced swelling and collapse of a polybase brush synthesized by atom transfer radical polymerization. *Soft Matter* **2006**, *2* (12), 1076-1080.
34. Adiga, S. P.; Brenner, D. W., Stimuli-Responsive Polymer Brushes for Flow Control through Nanopores. *J Funct Biomater* **2012**, *3* (2), 239-56.

35. de las Heras Alarcon, C.; Pennadam, S.; Alexander, C., Stimuli Responsive Polymers for Biomedical Applications. *ChemInform* **2005**, *36* (26), 276-285.
36. Gil, E. S.; Hudson, S. M., Stimuli-responsive polymers and their bioconjugates. *Progress in Polymer Science* **2004**, *29* (12), 1173-1222.
37. Jeong, B.; Gutowska, A., Lessons from nature: stimuli-responsive polymers and their biomedical applications. *Trends in Biotechnology* **2002**, *20* (7), 305-311.
38. Scott, R. C.; Crabbe, D.; Krynska, B.; Ansari, R.; Kiani, M. F., Aiming for the heart: targeted delivery of drugs to diseased cardiac tissue. *Expert Opin Drug Deliv* **2008**, *5* (4), 459-70.
39. Ju, E.; Li, Z.; Liu, Z.; Ren, J.; Qu, X., Near-infrared light-triggered drug-delivery vehicle for mitochondria-targeted chemo-photothermal therapy. *ACS Appl Mater Interfaces* **2014**, *6* (6), 4364-70.
40. Kurapati, R.; Raichur, A. M., Near-infrared light-responsive graphene oxide composite multilayer capsules: a novel route for remote controlled drug delivery. *Chem Commun (Camb)* **2013**, *49* (7), 734-6.
41. Yang, X.; Liu, X.; Liu, Z.; Pu, F.; Ren, J.; Qu, X., Near-infrared light-triggered, targeted drug delivery to cancer cells by aptamer gated nanovehicles. *Adv Mater* **2012**, *24* (21), 2890-5.
42. Song, L.; Ho, V. H.; Chen, C.; Yang, Z.; Liu, D.; Chen, R.; Zhou, D., Efficient, pH-triggered drug delivery using a pH-responsive DNA-conjugated gold nanoparticle. *Adv Healthc Mater* **2013**, *2* (2), 275-80.
43. Zan, M.; Li, J.; Luo, S.; Ge, Z., Dual pH-triggered multistage drug delivery systems based on host-guest interaction-associated polymeric nanogels. *Chem Commun (Camb)* **2014**, *50* (58), 7824-7.

44. Hu, B.; Du, H. J.; Yan, G. P.; Zhuo, R. X.; Wu, Y.; Fan, C. L., Magnetic polycarbonate microspheres for tumor-targeted delivery of tumor necrosis factor. *Drug Deliv* **2014**, *21* (3), 204-12.
45. He, H.; Sun, L.; Ye, J.; Liu, E.; Chen, S.; Liang, Q.; Shin, M. C.; Yang, V. C., Enzyme-triggered, cell penetrating peptide-mediated delivery of anti-tumor agents. *J Control Release* **2016**, *240*, 67-76.
46. Popat, A.; Jambhrunkar, S.; Zhang, J.; Yang, J.; Zhang, H.; Meka, A.; Yu, C., Programmable drug release using bioresponsive mesoporous silica nanoparticles for site-specific oral drug delivery. *Chem Commun (Camb)* **2014**, *50* (42), 5547-50.
47. Mitra, A. K.; Agrahari, V.; Mandal, A.; Cholkar, K.; Natarajan, C.; Shah, S.; Joseph, M.; Trinh, H. M.; Vaishya, R.; Yang, X.; Hao, Y.; Khurana, V.; Pal, D., Novel delivery approaches for cancer therapeutics. *J Control Release* **2015**, *219*, 248-268.
48. Andresen, T. L.; Thompson, D. H.; Kaasgaard, T., Enzyme-triggered nanomedicine: drug release strategies in cancer therapy. *Mol Membr Biol* **2010**, *27* (7), 353-63.
49. drug delivery reviews, H.-A. S., Stimuli-responsive polymers: Biomedical applications and challenges for clinical translation. *Advanced drug delivery reviews* **2013**.
50. Usov, D.; Gruzdev, V.; Nitschke, M.; Stamm, M.; Hoy, O.; Luzinov, I.; Tokarev, I.; Minko, S., Three-dimensional analysis of switching mechanism of mixed polymer brushes. *Macromolecules* **2007**, *40* (24), 8774-8783.
51. Ionov, L.; Minko, S., Mixed polymer brushes with locking switching. *ACS Appl Mater Interfaces* **2012**, *4* (1), 483-9.
52. Draper, J.; Luzinov, I.; Minko, S.; Tokarev, I.; Stamm, M., Mixed polymer brushes by sequential polymer addition: anchoring layer effect. *Langmuir* **2004**, *20* (10), 4064-75.

53. Sharma, S.; Johnson, R. W.; Desai, T. A., XPS and AFM analysis of antifouling PEG interfaces for microfabricated silicon biosensors. *Biosens Bioelectron* **2004**, *20* (2), 227-39.
54. Wang, H. Q.; Cheng, F.; Shen, W.; Cheng, G.; Zhao, J.; Peng, W.; Qu, J. P., Amino acid-based anti-fouling functionalization of silica nanoparticles using divinyl sulfone. *Acta Biomaterialia* **2016**, *40*, 273-281.
55. Dong, B. Y.; Manolache, S.; Wong, A. C. L.; Denes, F. S., Antifouling ability of polyethylene glycol of different molecular weights grafted onto polyester surfaces by cold plasma. *Polymer Bulletin* **2011**, *66* (4), 517-528.
56. Liu, L.; Li, W.; Liu, Q., Recent development of antifouling polymers: structure, evaluation, and biomedical applications in nano/micro-structures. *Wiley Interdiscip Rev Nanomed Nanobiotechnol* **2014**, *6* (6), 599-614.
57. Qian, Z. Y.; Li, S.; He, Y.; Liu, X. B., Synthesis and in vitro degradation study of poly(ethylene terephthalate)/poly(ethylene glycol) (PET/PEG) multiblock copolymer. *Polymer Degradation and Stability* **2004**, *83* (1), 93-100.
58. Altinisik, A.; Yurdakoc, K., Synthesis, Characterization, and Enzymatic Degradation of Chitosan/PEG Hydrogel Films. *Journal of Applied Polymer Science* **2011**, *122* (3), 1556-1563.
59. Kwon, H. J.; Lee, Y.; Phuong, L. T.; Seon, G. M.; Kim, E.; Park, J. C.; Yoon, H.; Park, K. D., Zwitterionic sulfobetaine polymer-immobilized surface by simple tyrosinase-mediated grafting for enhanced antifouling property. *Acta Biomater* **2017**, *61*, 169-179.
60. Li, W.; Liu, Q.; Liu, L., Amino acid-based zwitterionic polymers: antifouling properties and low cytotoxicity. *J Biomater Sci Polym Ed* **2014**, *25* (14-15), 1730-42.

61. Cao, B.; Li, L.; Wu, H.; Tang, Q.; Sun, B.; Dong, H.; Zhe, J.; Cheng, G., Zwitteration of dextran: a facile route to integrate antifouling, switchability and optical transparency into natural polymers. *Chem Commun (Camb)* **2014**, *50* (24), 3234-7.
62. Khalili, A. A.; Ahmad, M. R., A Review of Cell Adhesion Studies for Biomedical and Biological Applications. *Int J Mol Sci* **2015**, *16* (8), 18149-84.
63. Gardel, M.; Schwarz, U., Cell-substrate interactions. *J Phys Condens Matter* **2010**, *22* (19), 190301.
64. Matsuzaka, N.; Nakayama, M.; Takahashi, H.; Yamato, M.; Kikuchi, A.; Okano, T., Terminal-functionality effect of poly(N-isopropylacrylamide) brush surfaces on temperature-controlled cell adhesion/detachment. *Biomacromolecules* **2013**, *14* (9), 3164-71.
65. Cooperstein, M. A.; Canavan, H. E., Biological cell detachment from poly(N-isopropyl acrylamide) and its applications. *Langmuir* **2010**, *26* (11), 7695-707.
66. Nash, M. E.; Healy, D.; Carroll, W. M.; Elvira, C.; Rochev, Y. A., Cell and cell sheet recovery from pNIPAm coatings; motivation and history to present day approaches. *J Mater Chem* **2012**, *22* (37), 19376-19389.
67. Zakharchenko, A.; Guz, N.; Laradji, A. M.; Katz, E.; Minko, S., Magnetic field remotely controlled selective biocatalysis. *Nature Catalysis* **2017**, *1* (1), 73-81.

2. ROBUST, SOLVENT-FREE, CATALYST-FREE CLICK CHEMISTRY FOR THE GENERATION OF HIGHLY STABLE DENSELY GRAFTED POLY(ETHYLENE GLYCOL) POLYMER BRUSHES BY THE GRAFTING TO METHOD AND THEIR PROPERTIES<sup>1</sup>

---

<sup>1</sup> Laradji, A. M.; McNitt, C. D.; Yadavalli, N. S.; Popik, V. V.; Minko, S. Reprinted here with permission of publisher

## Abstract

Herein we report a robust, highly selective and efficient method to prepare dense polyethylene glycol (PEG) polymer brush on silicon substrates via solvent-free, catalyst-free, Strain-Promoted Acetylene-Azide Cycloaddition (SPAAC) reaction. First, poly(glycidyl methacrylate) was grafted to the silicon substrate as an anchoring layer to immobilize cyclopropanone-caged dibenzocyclooctyne-amine (photo-DIBO-amine) via an epoxy ring opening reaction providing protected and stable functionalized substrates. Next, three synthesized  $\alpha$ -methoxy- $\omega$ -azido-PEGs of different molecular weights (5, 10, and 20 Kg/mol) were successfully grafted on photo-DIBO-modified silicon substrates from melt after the deprotection of DIBO with UV-irradiation. PEG molecular weight, reaction temperature, and reaction time were all used to control the grafting reaction for targeted brush thicknesses and grafting densities. The highest grafting density obtained was close to 1.2 chain/nm<sup>2</sup> and was achieved when 5 Kg/mol PEG. The prepared PEG polymer brushes displayed efficient antifouling properties and stability in PBS buffer aqueous media for a period of at least two months.

**KEYWORDS:** polymer brush, grafting to, click chemistry, antifouling, brush stability

## 2.1. Introduction

Polymer brushes are tethered polymer chains by one end to a substrate where the polymer coils are forced to stretch away from the surface in order to avoid overlapping.<sup>1</sup> For the brush regime to exist, the following conditions are to be met: the brush height is greater and the distance between grafting point is less than two times of the radius of gyration of the polymer chain or  $h > 2(R_g^2)^{1/2}$ ,  $d < 2(R_g^2)^{1/2}$ , where  $d$  is the distance between the grafting points,  $h$  is the

brush height in a given solvent, and  $(R_g^2)^{1/2}$  is the radius of gyration of the same non grafted chain dissolved in the same solvent.<sup>2</sup> Grafted polymers have first drawn attention in the 1950s when their capabilities to deflocculate colloidal particles were realized.<sup>3</sup> Nowadays, and after over half a century of research, polymer brushes continue to fascinate and draw more interest which is clearly manifested in their wide range of applications in biomaterials and nanotechnology.<sup>4-11</sup>

Polymer brushes can be synthesized via two major approaches, namely the “grafting from” approach which relies on *in situ* polymerization from an initiator pre-immobilized on a substrate, and the “grafting to” approach when polymer chains are tethered to the surface via a chemical reaction between complementary functional groups of the polymer chains and the surface.<sup>12</sup> The latter approach implies that the polymer can be thoroughly characterized and optimized prior to its grafting, which results in well-defined and controlled polymer brushes.<sup>13</sup> This is the major advantage of the grafting to over the grafting from method when in the latter case molecular weight of the grafted chains is unknown and the grafted brush in many cases are polydisperse by molecular weight.

Various chemical reactions have been used and investigated to tether polymer chains to the surface of a substrate.<sup>14-21</sup> Among them, “click” reactions, are known for their simplicity, wide scope, high yielding, and above all high selectivity and orthogonality.<sup>22, 23</sup> Therefore, click reactions constitute very promising means to generate well-defined polymer brushes through the grafting to protocol. Azide-alkyne cycloadditions are a commonly used example of click reactions. They are catalyzed with Cu (I) and are, therefore, conducted almost only in solution. For example, Ostaci et al<sup>21</sup> have investigated the use of the copper(I)-catalyzed Huisgen 1,3-dipolar cycloaddition to graft polyethylene glycol to a silicon substrate. The grafting reaction

was carried out in THF and a relatively low polyethylene glycol (PEG) brush thickness of up to 6 nm was obtained after 72 h of reaction time. Grafting to process is limited by diffusion.<sup>13, 24</sup> Grafting in good solvent further slows down the grafting to due to the excluded volume effect. It was demonstrated with numerous examples that the grafting to method yields denser brushes if grafting is made in polymer melt.<sup>16, 24</sup> It is likely, that a click grafting to could be more efficient in melt vs solution process. Another drawback is associated with toxic Cu catalysts that could limits biological and biomedical applications of the brushes. Thus, the use of catalyst-free cycloaddition mechanism in polymer melt appears as an attractive way to yield densely grafted polymer brushes. To the best of our knowledge, using acetylene-azide cycloaddition to generate polymer brushes from melt has not been reported yet. It is the goal of the present work to report a detailed investigation on using solvent-free, catalyst-free, Strain-Promoted Acetylene-Azide Cycloaddition (SPAAC) reaction in order to synthesize PEG brushes by grafting to method. The reaction time and temperature, as well as the polymer molecular mass were varied to determine their effect on the grafted brush characteristics (thickness, density, and macroscopic morphology). Antifouling properties as well as stability of the PEG brushes in aqueous buffer media were assessed in the experiments.

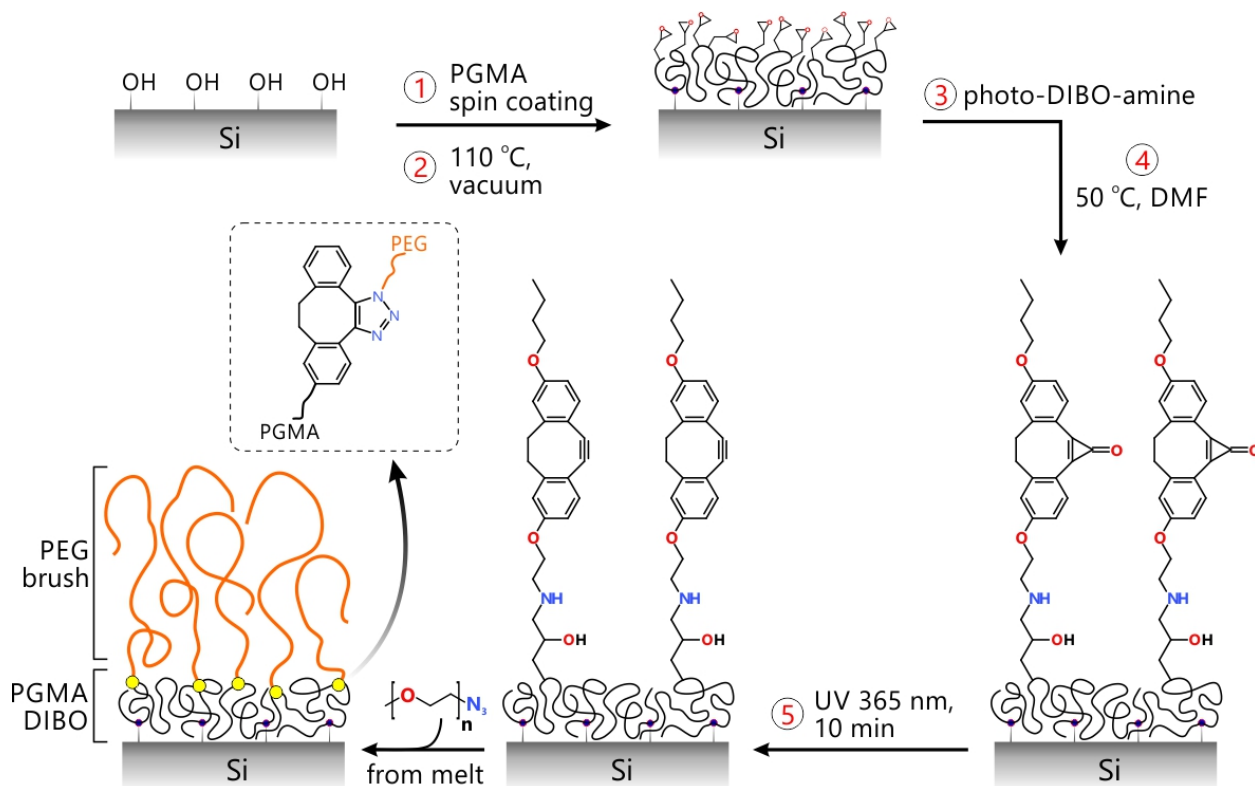


Figure 2.1. Preparation of PEG brushes via solvent-free, catalyst-free click reaction.

## 2.2. Experimental Section

**Materials.**  $\alpha$ -Methoxy- $\omega$ -azido-PEGs (PEG-N<sub>3</sub>) M<sub>n</sub> = 5, 10, and 20 Kg/mol were synthesized as previously reported<sup>25</sup> from methoxy poly(ethylene glycol) supplied by Sigma. *p*-Toluene sulfonyl chloride (98%), sodium azide (99.5%), Albumin-fluorescein isothiocyanate conjugate (BSA-FITC), and phosphate buffered saline (PBS, pH 7.4) were used as received from Sigma. Poly(glycidyl methacrylate) (PGMA) M<sub>n</sub> = 20 Kg/mol was used as received from Aldrich. Dimethylformamide (DMF) extra dry and anhydrous dichloromethane (DCM) were purchased from Acros Organics and Sigma-Aldrich consecutively. Cyclopropenone-caged dibenzocyclooctyne-amine (photo-DIBO-amine) was synthesized as previously described.<sup>26</sup> Silicon wafers (orientation 100, native oxide) were purchased from University Wafer (South Boston, MA, USA).

**Measurements.** Atomic Force Microscopy (AFM) images were obtained using Bruker Multimode Nanoscope instrument in the tapping mode. A spectrometric ellipsometer from Accurion (Germany) with a fixed angle of incidence of  $70^\circ$  was used to measure the dry films thickness of at three different locations of each sample. Ellipsometry thickness maps were generated using the Accurion software package, DataStudio. Fluorescence microscope Olympus BX51 was used for fluorescence visualization and the images obtained were processed using the software CellSens Dimension.

**Functionalization of Silicon Wafers with DIBO.** Silicon wafers were first cut into square pieces of  $1 \times 1 \text{ cm}^2$  and then sonicated in chloroform, DCM, and ethanol consecutively for 5 min each before being rinsed with DI water. The silicon wafers were then soaked in a solution of 28%  $\text{NH}_4\text{OH}$ /30%  $\text{H}_2\text{O}_2$ /DI water (1:1:1 by volume) for 1 hour at  $60^\circ\text{C}$  (Danger, the solution is highly oxidative and may cause chemical injury!). The substrates were rinsed with DI water and dried under a flux of Argon gas. Next, a solution of PGMA (0.25% in chloroform) was spin-coated (2500 rpm, 1500 rpm/s, 50 s) on the substrates and immediately annealed in oven at  $110^\circ\text{C}$  for 1 hour under vacuum. The resulting modified substrates were soaked in hot chloroform for 30 min to extract unreacted PGMA. Finally, photo-DIBO-amine (see Supporting Information) was immobilized on the PGMA layer by keeping the PGMA-modified silicon substrates in a solution of photo-DIBO-amine (12.5 mg/ml in DMF) at  $50^\circ\text{C}$  for 24 h. The obtained substrates were sequentially rinsed with DMF and chloroform and then dried with argon.

**Synthesis of PEG Brushes on the DIBO-Modified Silicon Wafers.** To graft PEG- $\text{N}_3$  chains, the photo-DIBO-modified silicon wafers were first subjected to a handheld UV lamp light from Spectroline model ENF-240C (365 nm wavelength, intensity of  $1 \text{ mW/cm}^2$ , held at a distance of

2 cm from the samples) for 5 to 10 minutes to expose the alkyne functional groups. Then, PEG-N<sub>3</sub> was spin-coated on the substrates and covered with a glass slide to avoid escape of the PEG melt and dewetting: the polymer melt was located between the substrate and the glass slide and holds at the place by capillary forces. The samples were annealed in oven under vacuum at different temperatures and for different times. To remove the unreacted PEG-N<sub>3</sub> chains, the samples were soaked in hot chloroform and water consecutively for 30 min each.

**Antifouling Properties of PEG Brushes.** Antifouling properties of the obtained brushes with three different molecular weights were assessed following a previously reported protocol.<sup>27</sup> Initially, the PEG brush modified substrates were equilibrated in PBS buffer (pH 7.4) for 2 hours and then immersed in a solution of BSA-FITC (0.25 mg/ml in PBS) at room temperature. 2 hours later, the substrates were rinsed with PBS buffer then DI water before being dried with argon. Fluorescence microscopy was next used to analyze the antifouling properties.

**PEG Brush Stability in PBS Buffer.** To assess their stability in aqueous media, the obtained PEG brush coated substrates were incubated in PBS buffer (pH 7.4) at room temperature. At various incubation times, the substrates were extracted and then immersed in a solution of BSA-FITC (0.25 mg/ml in PBS) for 2 hours at room temperature before being washed with PBS and water and finally dried with argon. The brush stability was assessed using fluorescence microscopy.

### **2.3. Results and Discussion**

**Functionalization of Silicon wafers with DIBO.** PGMA was used as a reactive anchoring layer to functionalize the surface of Si-wafers. It was deposited on the surface of the silicon substrates by spin-coating of a dilute solution of PGMA (0.25% in chloroform). The freshly deposited layer of about 35 nm thick, as measured by ellipsometry, was annealed for 1 hour at 110 °C under

vacuum yielding an average cross-linked film thickness of 6.4 nm after solvent rinsing and drying. In fact, it was previously reported that at these conditions only 5-7% of epoxy groups is lost upon PGMA annealing for up to 3 hours (depending on the amount of OH groups on the substrate).<sup>28</sup> The substrate surface was completely covered with smooth and homogeneous PGMA films, as shown by AFM microscopy (see supporting information, **Figure S1**). To prepare SPAAC-reactive surfaces, PGMA films were functionalized with photo-DIBO-amine. This cyclopropanone caged analog of DIBO has been chosen for one reason. While cyclooctynes are reasonably stable, they are known to be susceptible to nucleophilic attack.<sup>29-31</sup> DIBO, for example, undergoes relatively facile hydrolysis if heated in aqueous solutions, while photo-DIBO survives overnight refluxing in water (see Supporting Information, hydrolytic stability of DIBO/photo-DIBO). The functionalized samples with the protected DIBO can be conveniently stored for series of planned experiments. The progress of photo-DIBO-amine incorporation was monitored with ellipsometry since the PGMA film thickness increases with increased functionalization extent (**Figure 1**). In fact, increasing the polymer molecular weight results in thicker coatings,<sup>32</sup> and in our case the immobilized photo-DIBO molecules have caused the PGMA molar mass repeat unit to rise. As shown in figure 2.2, 24 hours was the duration of the reaction after which the PGMA film thickness increased by about 2 nm as detected by ellipsometry.

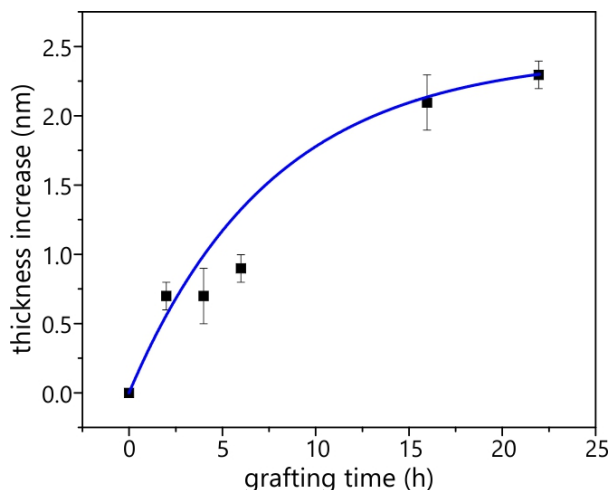


Figure 2.2. PGMA thickness increase upon photo-DIBO immobilization (the solid line is introduced for readers' convenience).

**Synthesis of PEG Brushes on DIBO-Modified Silicon Wafers.** The photo-DIBO-modified substrates were first exposed to UV light to deprotect the alkyne, then azide-terminated PEGs were clicked on the DIBO-modified substrates through the melting of an excess amount of PEG-N<sub>3</sub> chains (Error! Reference source not found.). The grafting kinetics of PEG-N<sub>3</sub> (5 Kg/mol) was investigated at 70, 100, and 130 °C. In all cases, it was observed that more than 50% of the brush thickness was achieved within the first 12 hours of the reaction, after which, the film thickness continued to grow though at a slower rate (Figure). This trend suggests that the kinetics during the first 12 hours was diffusion driven and the PEG-N<sub>3</sub> chains can smoothly diffuse to the PGMA-DIBO interface. Over 12 hours, the kinetics of grafting reaction decreases with time as the grafted PEG chains start to overlap creating a barrier that hinders the free PEG-N<sub>3</sub> from reaching the DIBO reactive groups and thus, it slows down PEG-N<sub>3</sub> diffusion.

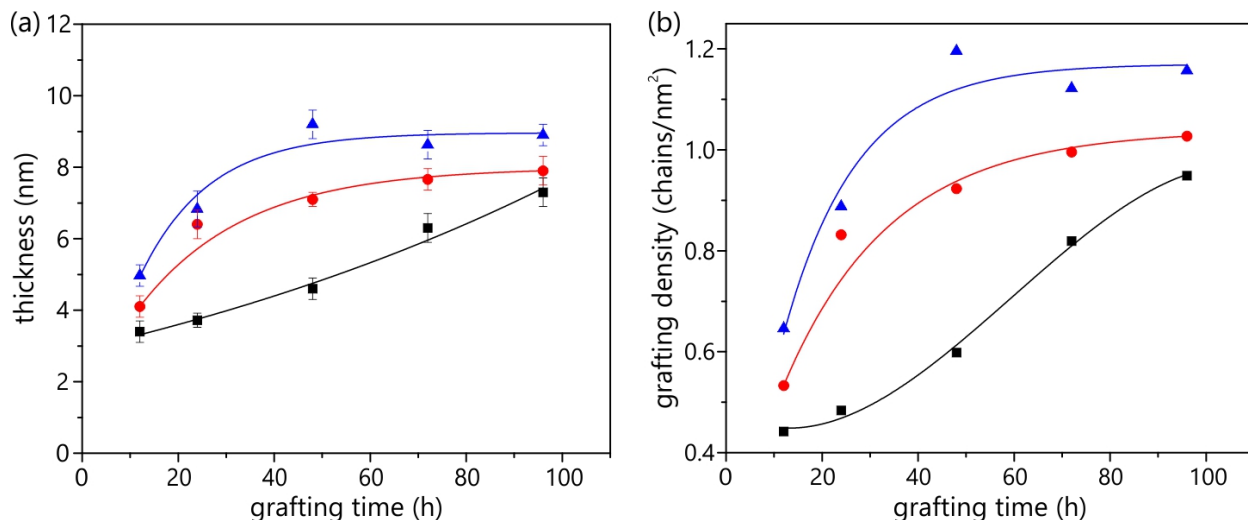


Figure 2.3. PEG films (from 5 Kg/mol) thickness (a) and grafting density (b) evolutions versus time at different temperatures [■ = 70 °C; ● = 100 °C; ▲ = 130 °C] (the solid lines are introduced for readers' convenience).

Similar observations have previously been reported.<sup>28, 33</sup> The grafting reaction at 130 °C yielded the highest PEG thickness obtained of about 9 nm after 96 hours. Indeed, PEG-N<sub>3</sub> chains diffusion increased with increasing temperatures. The grafting densities of the obtained PEG brushes were calculated from the average of three measurements of thicknesses using the following formula, assuming that the PEG density,  $\rho$ , is 1.09 g/cm<sup>3</sup>:  $\sigma = (h\rho N_a)/M_w$ ; where  $N_a$  is the Avogadro's number, and  $M_w$  the PEG molecular weight.

The effect of PEG-N<sub>3</sub> molecular weight on the resulting grafting density was also investigated. PEG-N<sub>3</sub> of 5, 10, and 20 Kg/mol were similarly melted at 130 °C on DIBO-modified substrates. The obtained PEG brush thickness was observed to increase from 9 to close to 12 nm and then decrease slightly below 9 nm as the PEG-N<sub>3</sub> molecular weight increased from 5 to 20 Kg/mol. However, the grafting density decreased as the molecular weight increased (Figure ). A combination of several factors is behind this experimental observation. One of them is the increase in polymer chains entanglement due to increasing PEG molecular weight, which decreases the diffusion. In fact, the maximum grafting density was obtained at PEG molecular

weight of 5 Kg/mol, which is only slightly higher than the PEG critical molecular weight of entanglement (4.4 Kg/mol).<sup>34</sup> Moreover, the higher excluded volume of larger polymer chains further hinders the close packing of the PEG chains resulting in higher distance between grafting sites.

Table 1 summarizes the measured and calculated PEG layers parameters, where, for all PEG-modified substrates, the radius of gyration of the polymer chains falls between the brush thickness (h) and the distance between the grafting sites (d), which indicates that the grafted layers are all in the brush regime and the polymer chains are densely packed.

Table 2.1. Characteristics of PEG brushes.

$M_w$ (Kg/mol)	h (nm)	$\sigma$ (chains/nm <sup>2</sup> )	$2(R_g^2)^{1/2}$ (nm)	d (nm)
5	8.9	1.16	5.04	1.05
10	11.5	0.748	7.14	1.31
20	8.7	0.283	10.1	2.12

$\sigma = (\rho Na)/M_w$ ,  $d = (4/\pi \sigma)^{1/2}$ ,  $(R_g^2)^{1/2} = b(N/6)^{1/2}$ , where a is the statistical segment length (b = 0.58 nm for PEG) and N is the degree of polymerization, for theta solvent.<sup>35</sup>

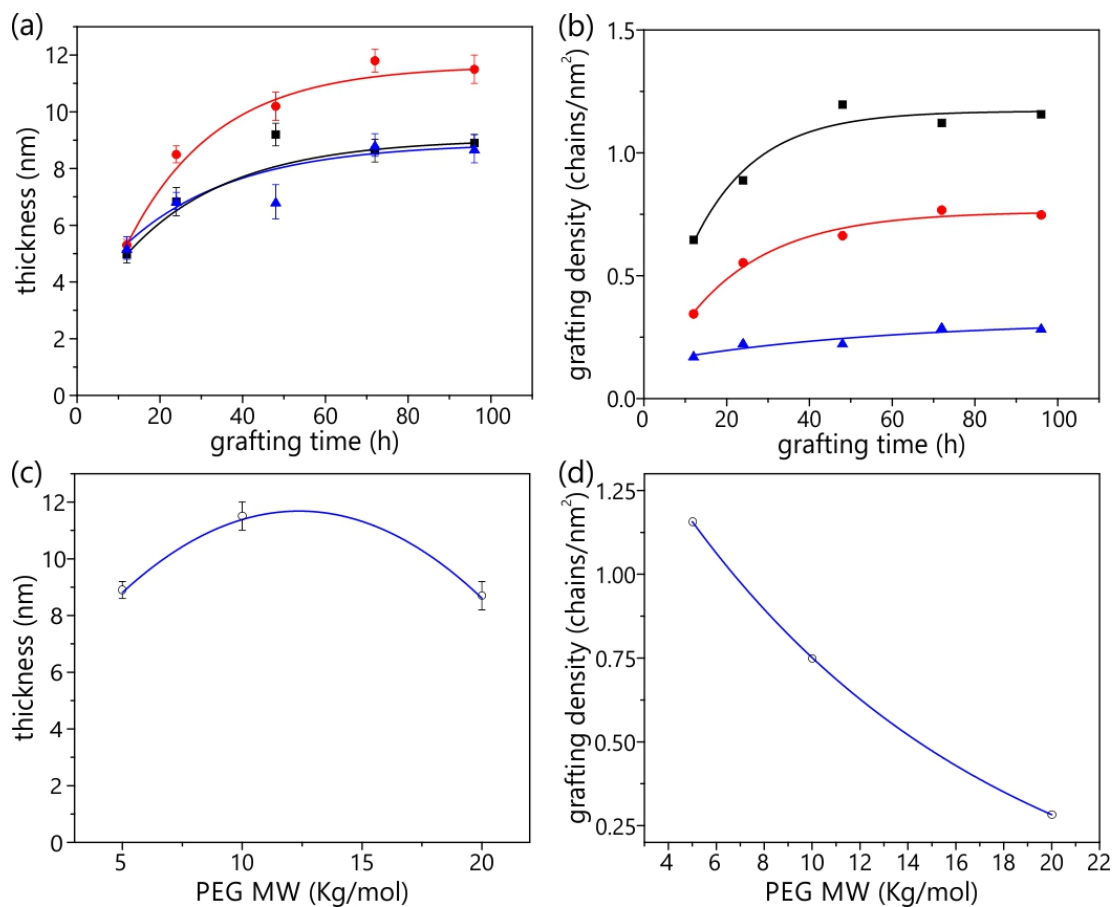


Figure 2.4. Effects of time and PEG Mn on films thickness (a, c) and grafting densities (b, d). [■ = 5 Kg/mol; ● = 10 Kg/mol; ▲ = 20 Kg/mol; ○ = grafting for 96 h at 130 °C] (the solid lines are introduced for readers' convenience).

The surface morphology of the resulting PEG brushes under ambient conditions was observed to be smooth and uniform (**Figure S1**). The step-by-step thickness map of the grafted layers (Figure ) further confirms the uniformity of the obtained brushes at a large scale where it is clearly seen that the variation in thickness height of the dry brush layers is less than 2 nm.

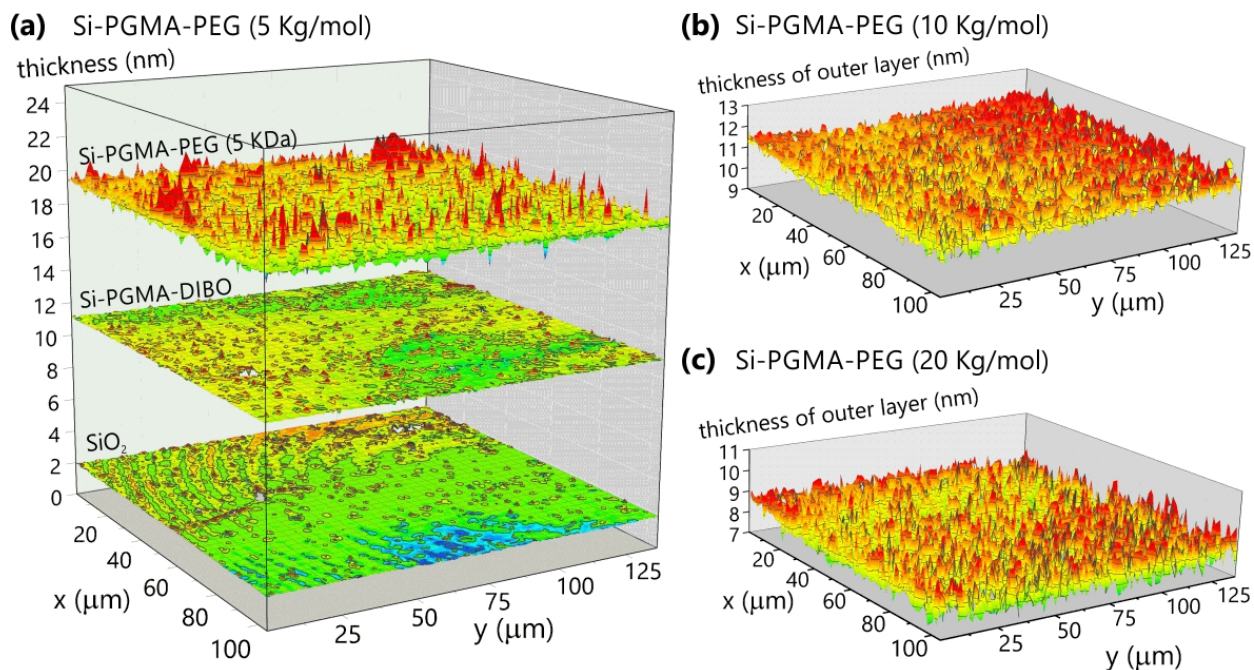


Figure 2.5. Step-by-step ellipsometric thickness maps of polymer brushes prepared from 5, 10, and 20 Kg/mol Mn of PEG on Si-wafers demonstrating the layers of silica (a), PGMA-DIBO (b) and PEG brushes (a-c).

**Antifouling Properties of PEG Brushes.** Biological substances, such as proteins, have the propensity to accumulate on surfaces. This tendency has its detrimental effects on, for example, medical devices that are embedded in the human body where, to avoid microbial influenced corrosion (MIC), replacing such devices is often required.<sup>36</sup> The grafting of antifouling polymers such as PEG is a commonly used method to keep biological organism away from colonizing medical implants. To evaluate the antifouling properties of the PEG-modified silicon wafers (with 5, 10, and 20 Kg/mol), here prepared, the substrates were immersed in a solution of BSA-FITC (0.25% in PBS buffer) for 2 hours. Fluorescence microscopy was subsequently used for the qualitative assessment of the amount of the BSA-FITC adsorbed. Compared to the control sample (no PEG), all layers with different size of PEGs were observed to repel protein efficiently, however, the protein adsorption was not observed to be dependent on the PEG molecular weight (Figure ). In terms of efficiency, this suggests that the nonspecific adsorption

of BSA is not affected within the studied range of molecular weight, mainly as the layers thicknesses are close to each other.

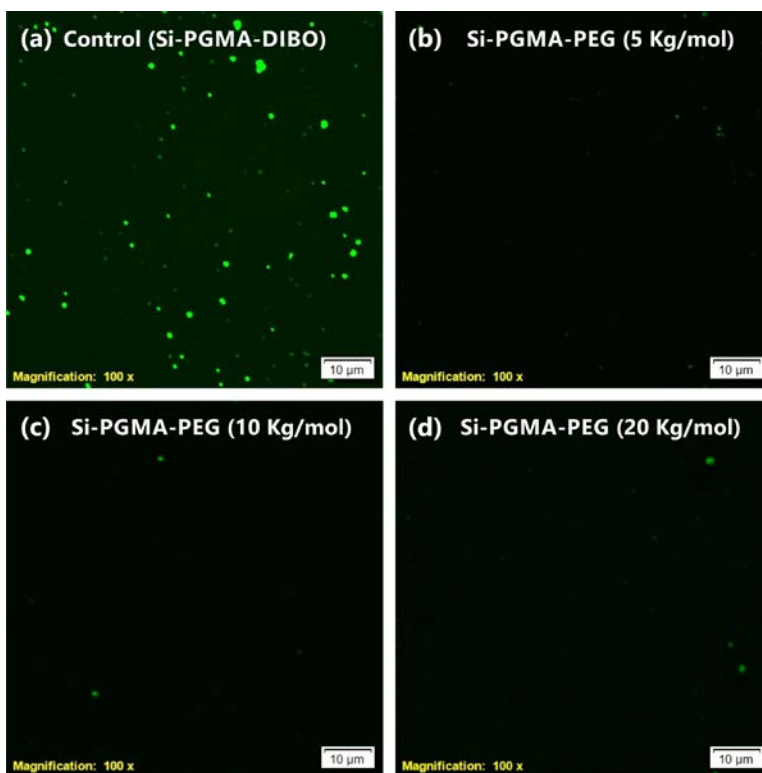


Figure 2.6. Fluorescence microscopy images of PEG brushes (from 5, 10, and 20 Kg/mol) after their incubation in a solution of BSA-FITC in PBS.

**PEG Brush Stability in PBS Buffer.** The stability of polymer brushes in aqueous media is a crucial prerequisite upon which hinges the successful use of its antifouling properties. For that purpose, synthesized polymer brushes from PEG (5 Kg/mol) were immersed in PBS buffer for a period of up to 2 months. The change in BSA adsorption on the substrates was used to evaluate the long term stability of the synthesized PEG polymer brushes.

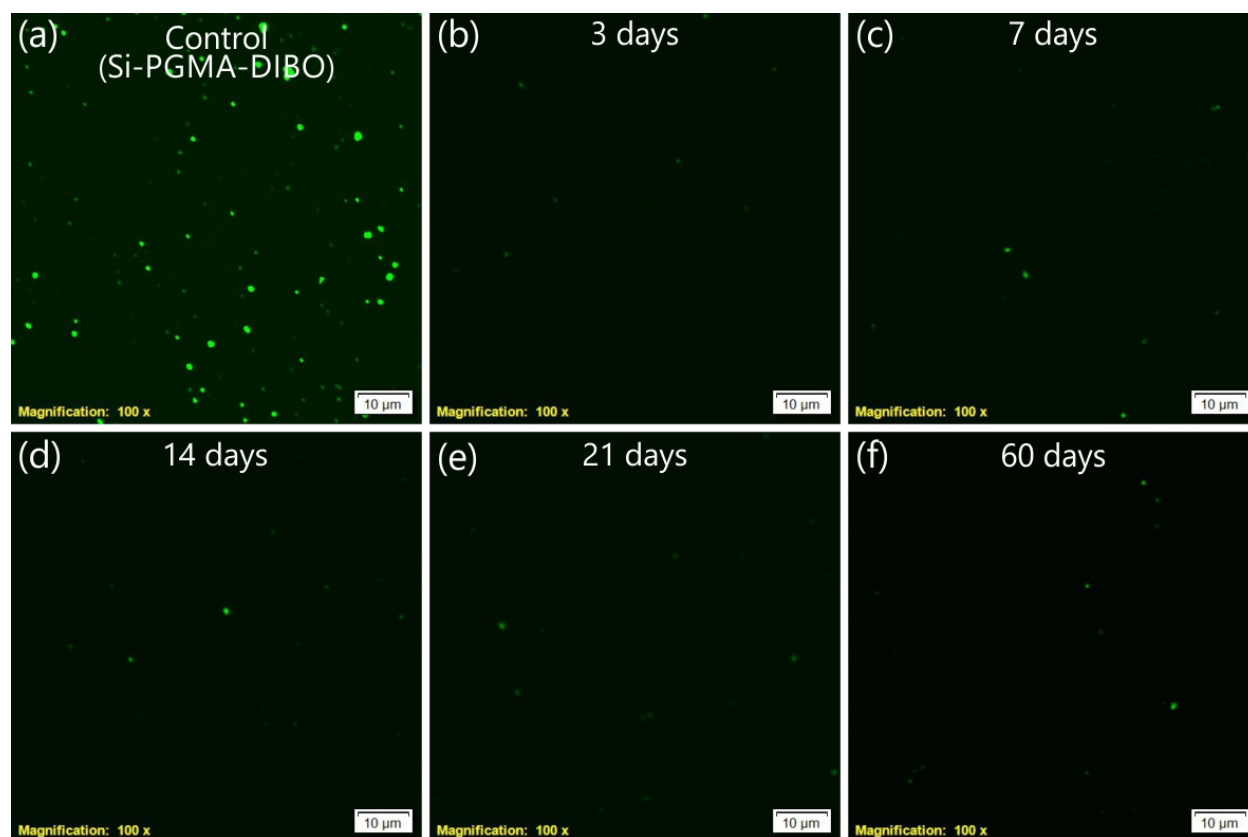


Figure 2.7. Fluorescence microscopy images of PEG films (5 Kg/mol) after incubation in PBS buffer for various periods.

Fluorescence microscope images of the adsorbed BSA on the substrates are shown in Figure . Throughout the period of investigation, the PEG-modified substrates antifouling properties were observed to persist for 60 days or longer which greatly exceeds those reported previously,<sup>37-40</sup> where all the polymer brush-modified substrates were observed to deteriorate within 40 days. The improved stability of the synthesized PEG brushes seems to be due to the cross-linked anchoring layer and the hydrophobic nature of the PGMA layer with its ability to shield the silicon substrate from water, thus, preventing Si-O-C bonds hydrolyses. These results seems to be in agreement with the work of Divandari et al.<sup>41</sup> Another factor that may have increased PEG brushes stability is the fact that PGMA-DIBO is about 9 nm thick where the grafting may take place across the film thickness. The latter will result in the 3D grafting effect where the brush

possesses self-healing properties.<sup>42</sup> According to the latter-mentioned mechanism, the degraded brush chains are “replaced” by chains previously hidden underneath the brush owing to the layered structure of the 3D-grafted brush. The stability of the brush in an aggressive environment is a valuable property for number of applications from antifouling<sup>43</sup> and dynamically changing surfaces<sup>44</sup> to electrochemical biosensors.<sup>45</sup>

## 2.4. Conclusion

Dense and macroscopically uniform PEG brushes were obtained using solvent-free, catalyst-free click chemistry grafting to method from melt. A grafting density of up to 1.2 chains/nm<sup>2</sup> was obtained using the described method. The grafting densities as well as the obtained thickness of PEG brushes were observed to be influenced by PEG molecular weight, temperature and time of the diffusion limited click reaction of the end-functionalized polymer. The PEG brushes obtained here possess high antifouling properties and above all were not observed to detach when stored in PBS aqueous media for a period of 2 months. It is anticipated that the grafting strategy here described can be applied to a broader range of polymers where a fairly high grafting density and selectivity are desired and with various inorganic substrates, such as, nanoparticles that often suffer from polymer chains detachment when stored in solvents for an extended period. The major advantage of the proposed method is a high stability of the functionalized surfaces, high selectivity and robustness of the grafting reaction.

## 2.5. References

1. Zhao, B.; Brittain, W. J. *Prog. Polym. Sci.* **2000**, 25, (5), 677-710.
2. Minko, S. *Polym. Rev.* **2006**, 46, (4), 397-420.
3. Brittain, W. J.; Minko, S. *J. Polym. Sci., Part A: Polym. Chem.* **2007**, 45, (16), 3505-3512.

4. Ayres, N. *Polym. Chem.* **2010**, 1, (6), 769-777.
5. Kwon, O. H.; Kikuchi, A.; Yamato, M.; Okano, T. *Biomaterials* **2003**, 24, (7), 1223-1232.
6. Wischerhoff, E.; Uhlig, K.; Lankenau, A.; Borner, H. G.; Laschewsky, A.; Duschl, C.; Lutz, J. F. *Angew. Chem., Int. Ed.* **2008**, 47, (30), 5666-8.
7. Chiang, E. N.; Dong, R.; Ober, C. K.; Baird, B. A. *Langmuir* **2011**, 27, (11), 7016-23.
8. Glinel, K.; Jonas, A. M.; Jouenne, T.; Leprince, J. r. m.; Galas, L.; Huck, W. T. S. *Bioconjugate Chem.* **2009**, 20, (1), 71-77.
9. Snaith, H. J.; Whiting, G. L.; Sun, B.; Greenham, N. C.; Huck, W. T.; Friend, R. H. *Nano Lett.* **2005**, 5, (9), 1653-7.
10. Pinto, J. C.; Whiting, G. L.; Khodabakhsh, S.; Torre, L.; Rodriguez, A. B.; Dalglish, R. M.; Higgins, A. M.; Andreasen, J. W.; Nielsen, M. M.; Geoghegan, M.; Huck, W. T. S.; Sirringhaus, H. *Adv Funct Mater* **2008**, 18, (1), 36-43.
11. Yameen, B.; Kaltbeitzel, A.; Langner, A.; Duran, H.; Muller, F.; Gosele, U.; Azzaroni, O.; Knoll, W. *J. Am. Chem. Soc.* **2008**, 130, (39), 13140-4.
12. Barbey, R.; Lavanant, L.; Paripovic, D.; Schuwer, N.; Sugnaux, C.; Tugulu, S.; Klok, H. A. *Chem. Rev.* **2009**, 109, (11), 5437-527.
13. Zdyrko, B.; Luzinov, I. *Macromol. Rapid Commun.* **2011**, 32, (12), 859-69.
14. Anne, A.; Demaille, C.; Moiroux, J. *Macromolecules* **2002**, 35, (14), 5578-5586.
15. Kingshott, P.; McArthur, S.; Thissen, H.; Castner, D. G.; Griesser, H. J. *Biomaterials* **2002**, 23, (24), 4775-85.
16. Luzinov, I.; Julthongpiput, D.; Malz, H.; Pionteck, J.; Tsukruk, V. V. *Macromolecules* **2000**, 33, (3), 1043-1048.

17. Roosjen, A.; van der Mei, H. C.; Busscher, H. J.; Norde, W. *Langmuir* **2004**, 20, (25), 10949-55.
18. Sudre, G.; Siband, E.; Hourdet, D.; Creton, C.; Cousin, F.; Tran, Y. *Macromol. Chem. Phys.* **2012**, 213, (3), 293-300.
19. Yang, Z. H.; Galloway, J. A.; Yu, H. U. *Langmuir* **1999**, 15, (24), 8405-8411.
20. Zdyrko, B.; Klep, V.; Luzinov, I. *Langmuir* **2003**, 19, (24), 10179-10187.
21. Ostaci, R. V.; Damiron, D.; Al Akhrass, S.; Grohens, Y.; Drockenmuller, E. *Polym. Chem.* **2011**, 2, (2), 348-354.
22. Kolb, H. C.; Finn, M. G.; Sharpless, K. B. *Angew. Chem., Int. Ed.* **2001**, 40, (11), 2004-2021.
23. Mocharla, V. P.; Colasson, B.; Lee, L. V.; Roper, S.; Sharpless, K. B.; Wong, C. H.; Kolb, H. C. *Angew. Chem., Int. Ed.* **2004**, 44, (1), 116-20.
24. Jones, R. A. L.; Lehnert, R. J.; Schonherr, H.; Vancso, J. *Polymer* **1999**, 40, (2), 525-530.
25. Deng, J. J.; Luo, Y.; Zhang, L. M. *Soft Matter* **2011**, 7, (13), 5944-5947.
26. Poloukhine, A. A.; Mbua, N. E.; Wolfert, M. A.; Boons, G. J.; Popik, V. V. *J. Am. Chem. Soc.* **2009**, 131, (43), 15769-76.
27. Tan, L.; Bai, L. C.; Zhu, H. K.; Zhang, C.; Chen, L. J.; Wang, Y. M.; Cheradame, H. *J. Mater. Sci.* **2015**, 50, (14), 4898-4913.
28. Popelka, S.; Houska, M.; Havlikova, J.; Proks, V.; Kucka, J.; Sturcova, A.; Bacakova, L.; Rypacek, F. *Eur. Polym. J.* **2014**, 58, 11-22.
29. Lo Conte, M.; Staderini, S.; Marra, A.; Sanchez-Navarro, M.; Davis, B. G.; Dondoni, A. *Chem Commun (Camb)* **2011**, 47, (39), 11086-8.

30. van Geel, R.; Pruijn, G. J.; van Delft, F. L.; Boelens, W. C. *Bioconjug Chem* **2012**, *23*, (3), 392-8.
31. Gobbo, P.; Mossman, Z.; Nazemi, A.; Niaux, A.; Biesinger, M. C.; Gillies, E. R.; Workentin, M. S. *J Mater Chem B* **2014**, *2*, (13), 1764-1769.
32. Soto-Cantu, E.; Lokitz, B. S.; Hiney, J. P.; Deodhar, C.; Messman, J. M.; Ankner, J. F.; Kilbey, S. M., 2nd. *Langmuir* **2011**, *27*, (10), 5986-96.
33. Kramer, E. J. *Isr. J. Chem.* **1995**, *35*, (1), 49-54.
34. Zdyrko, B.; Varshney, S. K.; Luzinov, I. *Langmuir* **2004**, *20*, (16), 6727-35.
35. Hammouda, B.; Ho, D. L. *J. Polym. Sci. Part B: Polym. Phys.* **2007**, *46*, 2196-2200.
36. Beech, I. B.; Sunner, J. A.; Arciola, C. R.; Cristiani, P. *Int. J. Artif. Organs* **2006**, *29*, (4), 443-52.
37. Branch, D. W.; Wheeler, B. C.; Brewer, G. J.; Leckband, D. E. *Biomaterials* **2001**, *22*, (10), 1035-1047.
38. Paripovic, D.; Klok, H.-A. *Macromol. Chem. Phys.* **2011**, *212*, (9), 950-958.
39. Fan, X.; Lin, L.; Messersmith, P. B. *Biomacromolecules* **2006**, *7*, (8), 2443-8.
40. Dalsin, J. L.; Hu, B. H.; Lee, B. P.; Messersmith, P. B. *J. Am. Chem. Soc.* **2003**, *125*, (14), 4253-8.
41. Divandari, M.; Dehghani, E. S.; Spencer, N. D.; Ramakrishna, S. N.; Benetti, E. M. *Polymer* **2016**.
42. Kuroki, H.; Tokarev, I.; Nykypanchuk, D.; Zhulina, E.; Minko, S. *Adv Funct Mater* **2013**, *23*, (36), 4593-4600.
43. Kuroki, H.; Tokarev, I.; Minko, S. *Ann. Rev. Mater. Res.* **2012**, *42*, 343-372.
44. Sheparovych, R.; Motornov, M.; Minko, S. *Adv. Mater.* **2009**, *21*, (18), 1840-+.

45. Zhou, J.; Tam, T. K.; Pita, M.; Ornatska, M.; Minko, S.; Katz, E. *ACS Appl. Mater. Interfaces* **2009**, 1, (1), 144-149.

3. A STIMULI-RESPONSIVE SWITCHABLE INTERFACE FOR MAMMALIAN CELLS  
STIMULATION AND CANCER CELLS DETECTION<sup>2</sup>

---

<sup>2</sup> Laradji, A. M.; Zhang, W.; McNitt, C. D.; Yadavalli, N. S.; Xie, J.; Popik, V. V.; and Minko, S. To be submitted to Biomaterials.

## **Abstract**

As a result of their dynamically changing interfacial properties, stimuli-responsive materials have the capability to present, capture, or release functional groups upon receiving external signals. Here in, we demonstrate that this property can be efficiently used to stimulate cell responses and mimic conditions for the adhesion and spreading of cells in the extracellular matrix. A patterned switchable interface made of the temperature-sensitive poly(N-isopropylacrylamide) and the cell adhesion peptide RGD (Arg-Gly-Asp) is first synthesized. Next, PNIPAM is stimulated to switch the surface properties from non adhesive at room temperature to cell adhesive at 37°C by hiding then presenting RGD to the cell adhesion integrin consecutively. Lowering the temperature back to RT causes the switchable interface to revert to its non fouling state, resulting in cells detachment. The cell attachment-detachment behavior here reported was applied in sorting cancer cells from a complex mixture of blood cells by targeting their over-expressed integrin molecules.

### **3.1. Introduction**

Many important cellular functions and behaviors are governed by the extracellular matrix (ECM). In fact, some functional molecules in the ECM carry biochemical information that trigger complex chain processes in mammalian cells. Of particular interest to the present article is the interaction between cell receptors integrins and cell-adhesive Arg-Gly-Asp (RGD) peptide that is found in many proteins of the ECM microenvironment. Cell adhesion integrins that are expressed by some cell types are widely known to recognize the motif RGD and effectively adhere to the matrix proteins carrying it.<sup>1-5</sup> The advanced understanding of this interaction and developments in nanotechnology have given rise to myriad designed biomaterials that aim at

regulating cellular responses and mimicking conditions for the growth and differentiation of cells in the ECM.<sup>6-8</sup>

Within the last decades, substantial advancements have been made in the understanding and development of polymer brushes. These surface-confined polymer chains, which stretch away from the surface at high enough grafting densities,<sup>9-10</sup> have already landed numerous applications in various fields such as nanomedicine,<sup>11-12</sup> sensors,<sup>13</sup> and textiles.<sup>14</sup> Furthermore, many research groups have explored using polymer brush-based materials to regulate integrin-RGD affinity.<sup>15-18</sup> Polymer brush patterning constitutes a more sophisticated approach to surface engineering of well-defined spatial distribution of polymer chains.<sup>19</sup> Through patterning of RGD clusters for example, cells adhesion was investigated by varying the clusters distance and spatial organization.<sup>8, 20</sup> Equally important to cells adhesion, cells detachment is essential in collecting adherent cells after culture and in cells sorting. Currently, trypsinization remains the most common means of cells detachment in culture. However, this approach often results in cell receptors damage,<sup>21</sup> which might affect cell function. To remediate this drawback, enzyme-free cell detachment using thermoresponsive PNIPAM brushes has been proposed. PNIPAM undergoes a reversible phase transition from hydrophilic to hydrophobic when its temperature is brought from under to above 32 °C. This switching behavior was explored to adhere cells at 37°C and induce cells detachment by simply lowering the environment temperature below 32 °C.<sup>22-24</sup> Furthermore, it was demonstrated that cells sorting from a complex cellular mixture can be achieved by tuning the adhesiveness of the substrate by mixing adhesive and non adhesive thermoresponsive polymers at different ratios.<sup>25</sup> Nevertheless, this approach may not be suitable for sorting target cells whose number is much smaller than the matrix cells, as in the case of the rare circulating tumor cells (CTC).

In this research project, we first report a facile synthesis of a patterned stimuli-responsive mixed polymer brush biomaterial of PNIPAM and RGD-conjugated polyacrylic acid (PAA) via two consecutive surface-initiated polymerization reactions and investigate its thermoresponsiveness below and above its LCST temperature of 32 °C. Next, the synthesized biomaterial was used to demonstrate its ability in switching fibroblast cells behavior between adhesion and detachment using temperature change as an external mild stimulus. Finally, the present biomaterial was applied to efficiently isolate U-87 MG cancer cells from mouse blood via the same concept.

### **3.2. Experimental Section**

**Materials.** N-Isopropylacrylamide (97%) was purchased from Sigma and was used after recrystallization from hexane. Tert-Butyl acrylate (98%), purchased from Sigma, was passed through inhibitors remover prior to its use. 2-azidoethyl 2-bromoisobutyrate, sodium azide, and phosphate buffered saline (PBS, pH 7.4) were used as received from Sigma. Poly(glycidyl methacrylate) (PGMA) 20 Kg/mol was used as received from Aldrich. Dimethylformamide (DMF) extra dry and anhydrous dichloromethane (DCM) were purchased from Acros Organics and Sigma-Aldrich consecutively. Dibenzocyclooctyne-amine (DIBO-amine) was synthesized as previously described.<sup>26</sup> The peptide RGDS was purchased from Cayman Chemical. Silicon wafers (orientation 100, native oxide) were purchased from University Wafer (South Boston, MA, USA).

**Measurements.** Atomic Force Microscopy (AFM) images were obtained using Bruker Multimode Nanoscope instrument in the tapping mode. A spectrometric ellipsometer from Accurion (Germany) with a fixed angle of incidence of 70° was used to measure the dry films thickness of at three different locations of each sample. Ellipsometry thickness maps were

generated using the Accurion software package, DataStudio. A fluorescence microscope (Olympus BX51) was used for fluorescence visualization.

**Functionalization of Silicon Wafers with DIBO.** The immobilization of photo-DIBO on the surface was done as we previously reported.<sup>27</sup> Briefly, silicon wafers were first cut into square pieces of 1x1 cm<sup>2</sup> and then sonicated in chloroform, DCM, and ethanol consecutively for 5 min each before being rinsed with DI water. The silicon wafers were then soaked in a solution of 28% NH<sub>4</sub>OH/30% H<sub>2</sub>O<sub>2</sub>/DI water (1:1:1 by volume) for 1 hour at 60 °C (caution, the solution is highly oxidative and may cause chemical injury!). The substrates were then rinsed with DI water and dried under a flux of Argon gas. Next, a solution of PGMA (0.1% in chloroform) was spin-coated (2500 rpm, 1500 rpm/s, 60 s) on the substrates and immediately annealed in oven at 110 °C for 1 hour under vacuum. The resulting modified substrates were soaked in hot chloroform for 30 min to extract unreacted PGMA. Finally, photo-DIBO-amine was immobilized on the PGMA layer by keeping the PGMA-modified silicon substrates in a solution of photo-DIBO-amine (12.5 mg/ml in DMF) at 50 °C for 24 h. The obtained substrates were sequentially rinsed with DMF and chloroform and then dried with argon.

**Poly (N-isopropylacrylamide) (PNIPAM)-Patterns Generation.** A TEM grid (12.5 pitch) was used as a photomask to expose select regions of the Photo-DIBO modified silicon wafers to a hand-held UV light from Spectroline<sup>®</sup> with a wavelength 365 nm and an intensity of 1mW/cm<sup>2</sup> for 150 seconds. Next, the substrates were immersed in a solution of 2-Azidoethyl 2-bromoisobutyrate (5% in DMF V/V) for 1 hour at room temperature to attach the ATRP initiator on the deprotected areas of the photo-modified substrate. PNIPAM patterns on the slides were generated through a grafting from procedure usingARGET ATRP according to the following protocol: the initiator-modified surfaces were immersed into a solution containing 700 µl of

methanol, 300  $\mu$ l of DI water, 450 mg of NIPAM, 9  $\mu$ l Cu(II)Br (50 mg/ml in DI water), and 9  $\mu$ l PMDTA (10% in DI water). After homogenization, the polymerization reaction was immediately started upon the addition of 50  $\mu$ l of ascorbic acid (40 mg/ml) into the solution. The polymerization reaction was conducted at room temperature and was stopped, at different times (according to desired thicknesses), by exposing the reaction mixture to air. Finally, the patterned slides were rinsed with ethanol and then DI water before being dried with a stream of argon.

**Polyacrylic Acid Patterning and RGDS Immobilization.** The PNIPAM patterned slides were first immersed in a solution of sodium azide (40 mg/ml in DI water for 30 minutes) in order to convert the bromine end groups of PNIPAM chains into azide to avoid tert-butyl acrylate copolymerization from PNIPAM end-chains. Next, the ATRP initiator was immobilized as described above after exposing the remaining alkyne groups by UV light. To generate polyacrylic acid brushes from the slides the following protocol was used: the initiator-modified slides were immersed in a solution made of 1.5 ml of ethanol, 500  $\mu$ l of tert-butyl acrylate, 9  $\mu$ l Cu(II)Br (50 mg/ml in DI water), and 9  $\mu$ l PMDTA (10% in DI water). Similarly to before, the polymerization was initiated right after adding 50  $\mu$ l of ascorbic acid (40 mg/ml) into the solution. The slides were then washed with ethanol and dried with argon. Finally, the slides were immersed in a solution of methanesulfonic acid (1.5% in extra dry dichloromethane) for 2 minutes at room temperature to remove the pendant tert-butyl groups of poly (tert-butyl acrylate) and yield polyacrylic acid (PAA) brushes. An amidation reaction between the carboxylic groups of PAA with the primary amine groups of RGDS was, ultimately, performed to immobilize RGDS peptides onto the PAA brushes in presence of EDC and NHS simultaneously to activate the acrylic acid groups.

**Cell Culture.** NIH/3T3 murine fibroblasts and U-87MG human glioblastoma cells were purchased from ATCC. NIH/3T3 and U-87MG cells were cultured in DMEM medium (Corning, USA) with 10% FBS (Corning, USA), 1% nonessential amino acids, and 1% penicillin-streptomycin (MediaTech, USA). The cell line was incubated humidly under 37 °C and 5% CO<sub>2</sub>.

**NIH/3T3 Cells Attachment-Detachment Sequence.** PNIPAM-patterned substrates were deposited on a 6-well plate. Before seeding cells, the substrates were submerged in 75% ethanol solution overnight for sterilization purpose. Then, the ethanol solution was removed and the substrates were further rinsed with PBS for three times.  $3 \times 10^5$  NIH/3T3 cells were seeded onto the substrate in each well. Cells were incubated humidly under 37 °C and 5% CO<sub>2</sub> for 24 hours, and then stained with calceinAM.

**Cell Preparation for Cancer Cells Sorting.** U-87MG cells expressing endogenous integrin  $\alpha\beta$  were selected as the model cancer cells for sorting test. When reaching 80-90% confluency, U-87MG cells were labeled with CFSE cell labeling agent (Abcam) and then collected via trypsinization. The cells were fixed in 2% formaldehyde solution in PBS (50% formalin solution) overnight at 0-4 °C. Then U-87MG cells were counted using hemocytometer and further stained with DAPI (Sigma-Aldrich). During the whole process, cells were kept at 0-4 °C and protected from direct light exposure. Blood cells were collected from female balb/c mice. Briefly, the whole blood was collected and mixed with heparin solution (1000 U/mL in PBS). The whole blood mixture was centrifuged to separate blood cells from serum. Blood cells were carefully rinsed with cold PBS for twice, then fixed with 2% formaldehyde solution in PBS (50% formalin solution) overnight at 0-4 °C. Blood cells were counted using hemocytometer. To prevent any heat induced damage, cells were kept at 0-4 °C during the preparation process.

### 3.3. Results and Discussion

**PNIPAM-Patterned Substrates.** Silicon wafers were modified with PGMA upon which photo-DIBO molecules were immobilized. Photo-DIBO molecules were used to attach an ATRP initiator to select areas after the surface was covered with a TEM grid and exposed to a UV light. The initiator-coated substrates were subsequently used to generate patterned thin film of PNIPAM viaARGET ATRP. As shown in figure 3.1, the polymerization reaction was a controlled process. In fact, the thickness was observed to increase linearly with the polymerization time.

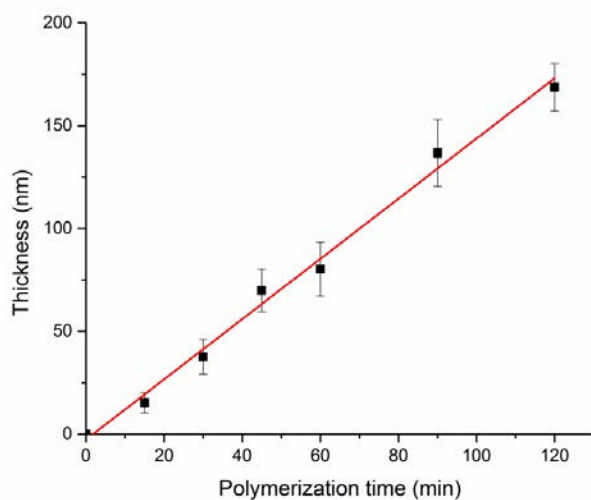


Figure 3.1. Fitted curve of NIPAMARGET ATRP kinetics from substrate-coated initiators.

The patterned polymer brush was imaged by AFM. As seen in figure 3.2, the formed patterns are highly organized and smooth. In this image, the height profile from AFM indicates a uniform thickness of about 80 nm around the scanned area.

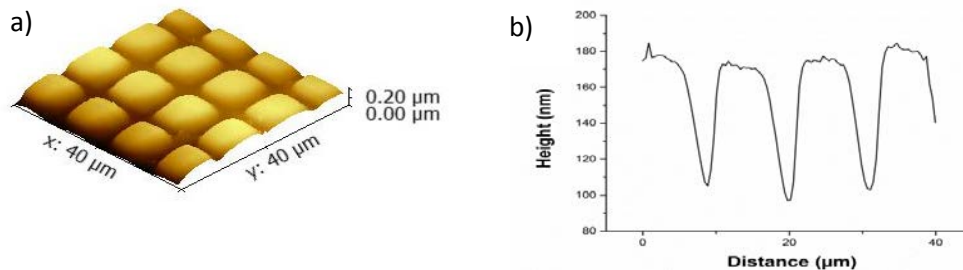


Figure 3.2. AFM morphology (a) and thickness profile (b) of the PNIPAM brush (80 nm) in dry.

Using two complementary techniques, the thermoresponsiveness of several thicknesses of the patterned polymer brushes was next investigated in PBS buffer (pH 7.4) at different temperatures. Figure 3.3 reports the ellipsometric angles ( $\psi$  and  $\Delta$ ), and the thickness change of PNIPAM films as the temperature increases from 15 °C to 42 °C. In all cases, it is observed that the transition is not spontaneous but rather extends over 8-10° C. PNIPAM is known to exhibit a lower critical solution temperature (LCST) in aqueous media. When PNIPAM chains are confined to a surface, the polymer chains collapse and become less hydrophilic as the temperature increases. In our case this transition seems to depend on the thickness in the dry state as it is noticed that higher thicknesses generate higher thermal responsiveness. AFM images (figure 3.4) further confirm the ellipsometric measurement, as it can be seen that PNIPAM brush thickness changes from 80 nm to 220 nm when the temperature changes from above to below the LCST.

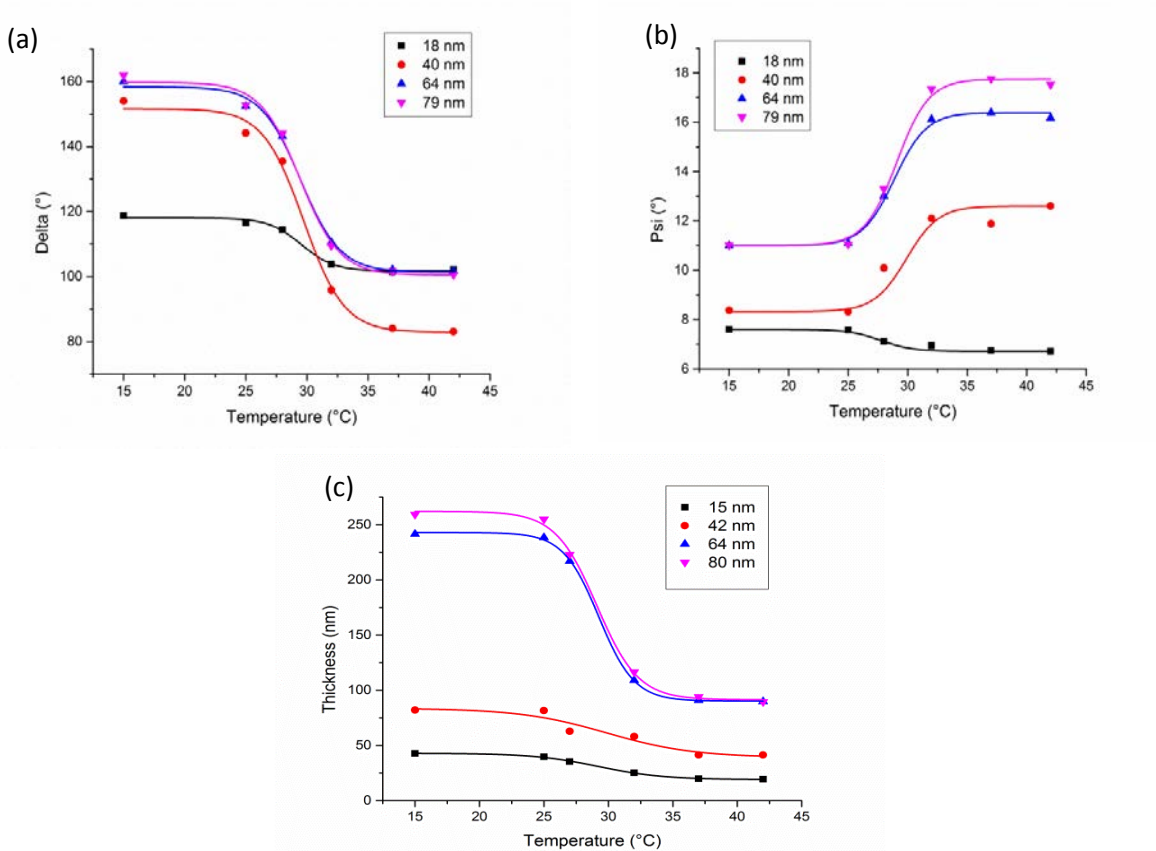


Figure 3.3. Ellipsometric  $\Delta$  (a),  $\Psi$  (b) changes and thickness (c) changes with temperature.

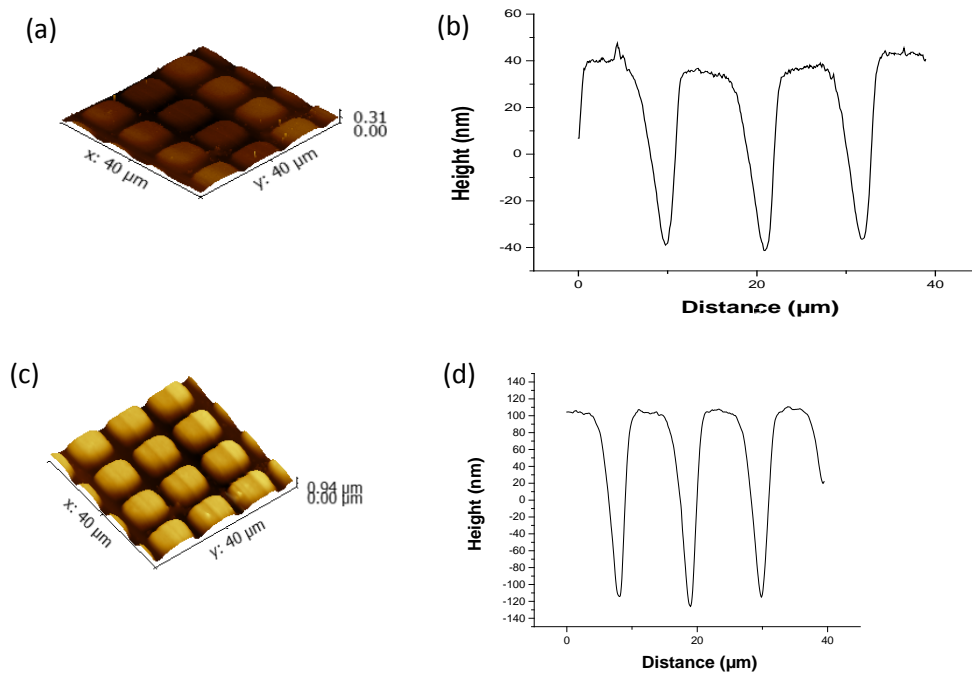


Figure 3.4. AFM images and height profile of PNIPAM thickness characterizing thickness change with temperature above (a, b) and below (c, d) the LCST.

**Polyacrylic Acid and RGDS Patterning.** PtBA patterning was first achieved with target ATRP in ethanol. The reaction conditions were chosen to achieve a slow increase in PtBA thickness with time to have a better control. One hour after the polymerization reaction, PtBA thickness was ~16.9 nm (ellipsometry). After acid hydrolysis of the PtBA, the thickness decreased to 8.9 nm in dry state. Swelling in PBS buffer of the mixed polymer brush (PNIPAM-PAA) is shown in figure 3.5. Polyacrylic acid is a pH-responsive polyelectrolyte. At the pH of 7.4, the polymer chains are expected to stretch away from the surface as they are fully solvated. In our case, PAA film thickness increased from 8.9 nm to ~110 nm (figure 5b), which brought the thickness of PNIPAM and PAA to the same level. However, the thickness difference between the two polymers reached 100 nm when the temperature was lowered below the LCST of PNIPAM. RGDS immobilization on PAA chains was achieved through a simple EDC coupling between the carboxylic groups of PAA and the amine groups of RGDS. Upon the immobilization reaction, the thickness increased from 8.9 nm to 17.3 nm. PAA and PAA-RGDS thicknesses in different states are summarized in table 3.1.

Table 3.1. PAA and PAA-RGD thicknesses (in nm) in air and liquid.

	<b>PAA</b>		<b>PAA-RGDS</b>	
	Air	swollen state	Air	swollen state
<b>Ellipsometry</b>	8.9 ± 0.4	111.9 ± 8.5	17.3±1.7	118.6±4.1
<b>AFM</b>	9.6	106	20	110

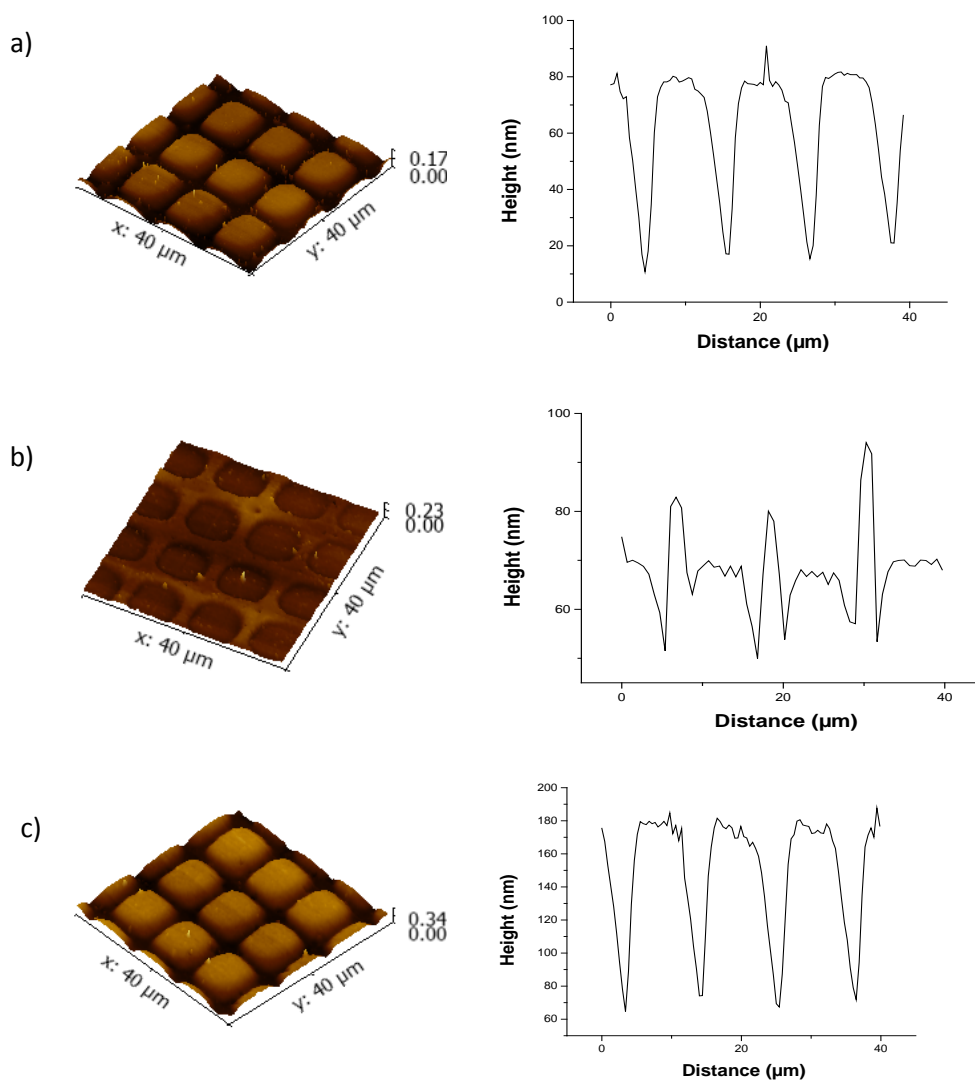


Figure 3.5. AFM of PNIPAM-PAA brushes in dry (a), collapsed (b) and swollen state (c).

**Fibroblast Cells Adhesion and Detachment.** Fibroblast cells were seeded on four different substrates for 24 hours. Four samples of different thicknesses (0, 18, 80, and 150 nm) were used to investigate the thickness effects on cells adhesion. As seen from figure 3.6, the number of cells attached does depend on the thickness of PNIPAM. Cells attachment to the substrates slightly increases with a decreasing thickness of PNIPAM between 0 and 80 nm, however, at a thickness of 150 nm, a very low number of cells were able to attach to the substrate. The latter case is clearly manifested by the shapes of 3T3 cells that remained round. Cells that exhibit that

shape do not have their integrins involved in any attachment and are rather held by physical interactions with the substrate.<sup>28</sup> 3T3 cells spreading, on the other side, signals strong bonding interactions between cells integrins and RGD as the cells extend and occupy the maximum possible area. Furthermore, since cells are seeded on a patterned biointerface that alternate between adhesive (5  $\mu\text{m}$ ) and non adhesive (7.5  $\mu\text{m}$ ) areas, it is evident that cells are able to bridge multiple ( $\geq 3$ ) non adhesive regions. It was previously shown that cell spreading becomes limited when a maximum non adhesive area is crossed.<sup>29</sup> Though this observation depends on other factors such as the area of the RGD clusters, in our case, however, this outcome was not observed.

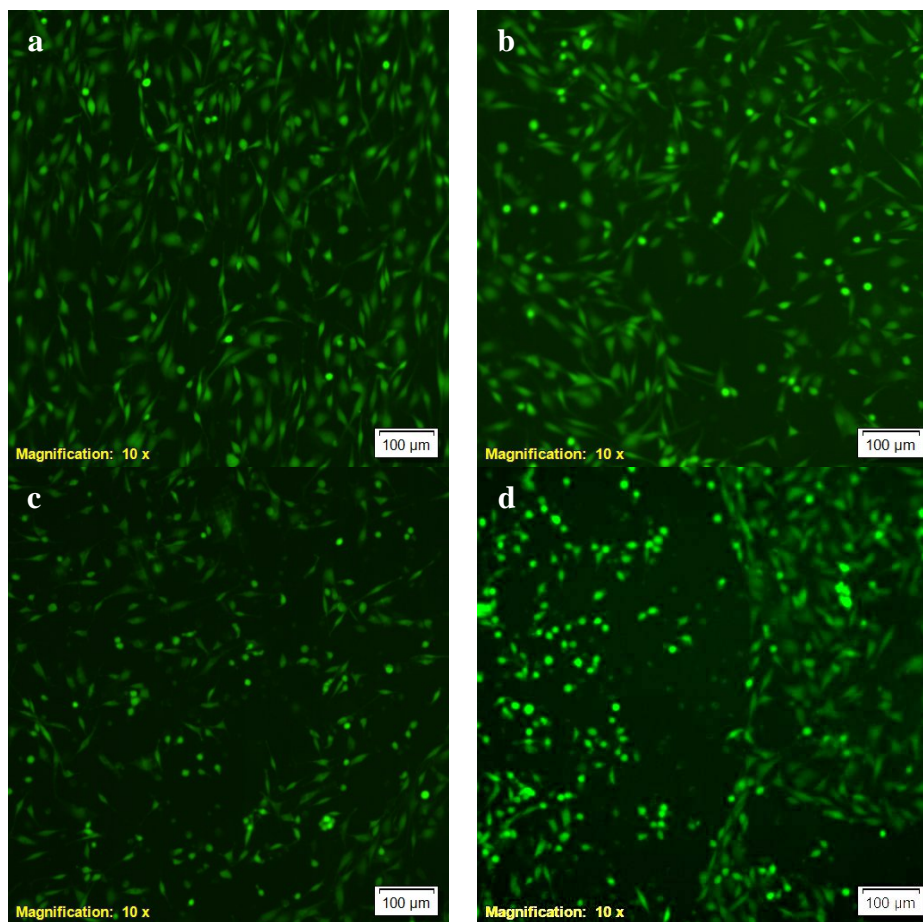


Figure 3.6. 3T3 cells attached to PNIPAM thickness (nm) of: 0 (a), 18 (b), 80 (c), and 150 (d).

The non attachment of 3T3 cells on substrates with PNIPAM of 150 nm thickness is likely due to the non accessibility of RGD to cells integrins. This observation seems to correlate well with the theoretical studies done by Halperin et al<sup>30</sup> although the substrates are slightly different. In their work, adhesion was suggested to be more pronounced when the RGD height position ( $z$ ) falls between  $h(37\text{ }^\circ\text{C}) - L_I$  and  $h(37\text{ }^\circ\text{C})$ , with  $h(37\text{ }^\circ\text{C})$  represents PNIPAM thickness at  $37\text{ }^\circ\text{C}$  and  $L_I$  ( $\sim 20\text{ nm}$ ) is the distance between RGD and the cell surface. In our biointerface RGD location (110 nm by AFM) is rather lower than  $h(37\text{ }^\circ\text{C}) - L_I$  which is at least 130 nm, which makes it non reachable by cells integrins.

The detachment of 3T3 cells from the substrates were achieved by lowering the cell medium

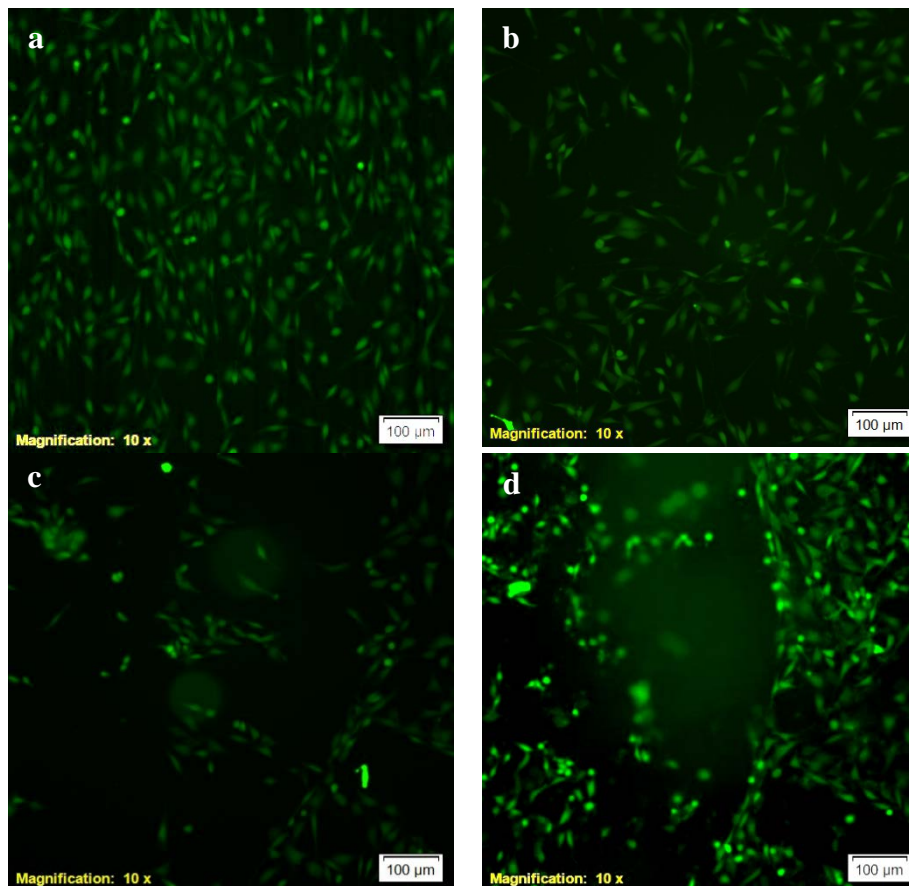


Figure 3.7. Cells release From PNIPAM thickness (nm) of: 0 (a), 18 (b), 80 (c), and 150 (d).

temperature to room temperature (below PNIPAm LCST). Figure 3.7 shows the correlation between PNIPAm layer thickness and extent of cells detachment. After a cooling period of 1 hour, 3T3 cells were not observed to detach from the control sample (with no PNIPAm) and the number of cells remained unchanged. The extent of cells detachment was a little higher when a PNIPAm layer of 18 nm was used, and the highest when an 80 nm of PNIPAM thickness was used. In the latter case, the extension of PNIPAM chains, which substantially reduces RGD accessibility, and their hydrophilicity, which caused cells to lose their tension on the substrates, disrupted integrin-RGD bonds and caused the cells to lose the focal adhesion and detach ultimately.

**Cancer Cells Isolation.** Approximately 90% of cancer-related deaths are attributed to the poorly understood tumor metastasis in lieu of primary tumors.<sup>31</sup> Metastasis is believed to be caused by the spreading of circulating tumor cells (CTCs) from the primary tumor site to distant organs through the blood.<sup>32</sup> The proposed CTC detection platform constitutes a better alternative approach to detect and isolate cancer cells based on their overexpression of certain biomolecules. For example, many cancer cells are marked with an overexpression of the cell adhesion integrin,<sup>33-34</sup> and more specifically integrin  $\alpha\beta3$ .<sup>35</sup> In this study, we have already shown how 3T3 cells adhesion and detachment from our switchable interface can be controlled remotely by changing the medium temperature. Using the same concept, we investigated the isolation of U-87 MG cancer cells from mouse blood. From one side, U-87 MG cells are known to exhibit one of the highest integrin overexpression.<sup>36</sup> On the other hand, blood cells (BC) do express the cell adhesion integrin on their surface as in the case of white blood cells and blood platelets; however, these integrins need to be activated before mediating any adhesion.<sup>37</sup>

Initially, the switchable interface was immersed in a PBS buffer (pH 7.4) solution containing either U-87MG cells or blood cells to investigate their adhesion separately.

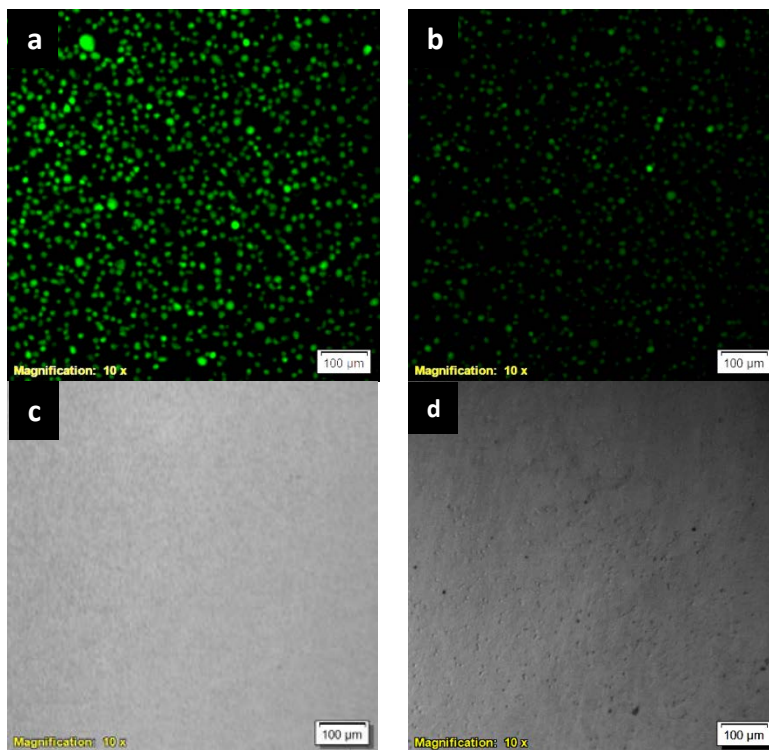


Figure 3.8. Adhesion and detachment of U-87MG cells (a) and blood cells (b).

Figure 3.8 shows that both cancer cells and blood cells seem to interact with the substrate upon an incubation period of 9 hours at 37 °C. After a cooling period of 1 hour at room temperature, most cancer cells remained attached to the surface, unlike blood cells. With bright field microscope (data not shown), it was confirmed that cancer cells did attach on the surface via the integrin-RGD interaction as the cells were observed to adopt a flat shape. As reviewed previously,<sup>28</sup> cells flattening during static in-vitro cell adhesion is a consequence of integrin bonding. However, blood cells interactions with the substrate were likely weak.

In the next experiment, the switchable biointerface was immersed in PBS buffer (pH 7.4) containing U-87 MG cancer cells and blood cells at a ratio of 1/1000 (U87/ BCs). During the incubation period of 9 hours, the medium temperature was oscillated between 37 °C and 25 °C for one hour during each period. A separate sample was incubated with the same mixture of cells and for the same period but with no temperature fluctuation. As shown in figure 3.9 a-e, U-87MG cells number did increase with every heating and cooling sequence to reach a maximum at 9 hours that corresponds to  $\geq 90$  % cells recovery (figure 3.10). Recovery of U-87MG cells, was however, much lower when the medium temperature remained at 37 °C during the whole incubation period (figure 3f).

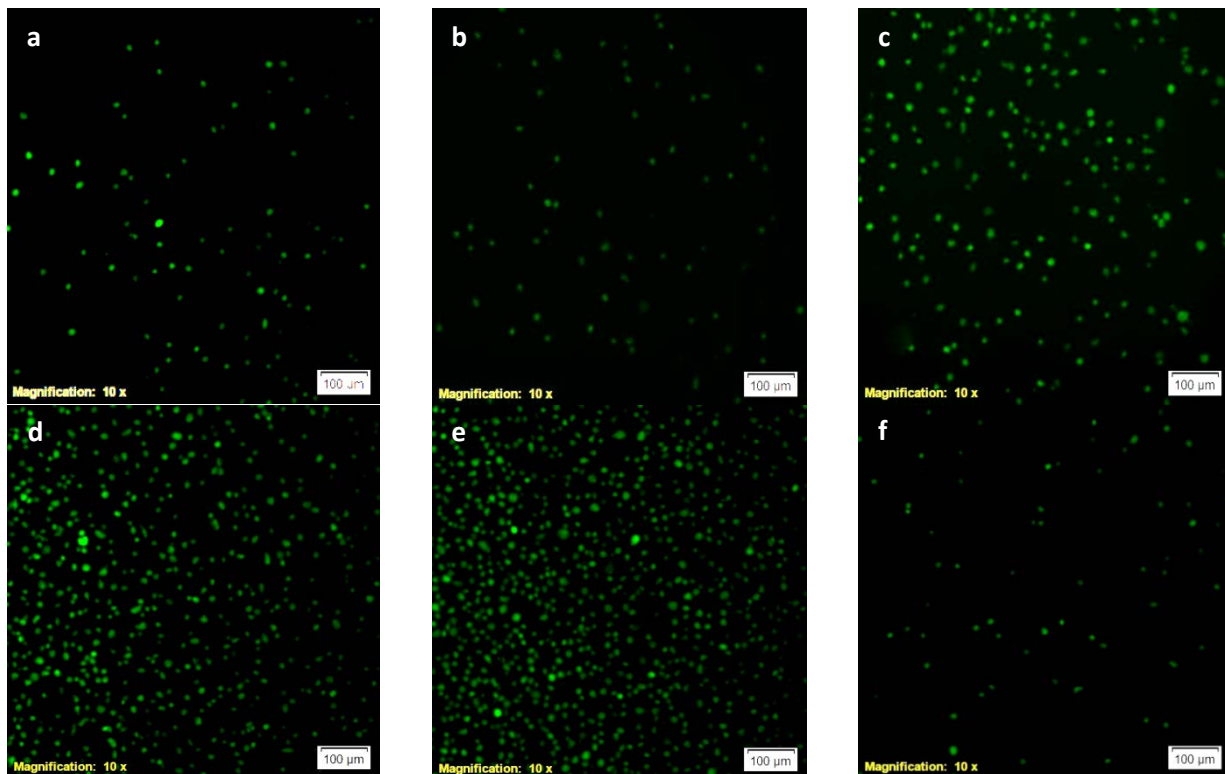


Figure 3.9. U-87MG cells separation by temperature oscillation (a-e) and continuous (f).

It is clear from these results that the repeated sequence of heating and cooling of the substrates enabled the isolation of more cells concentration as blood cells are released from the substrate upon cooling to recruit more of the strongly adhering U-87 MG cells.

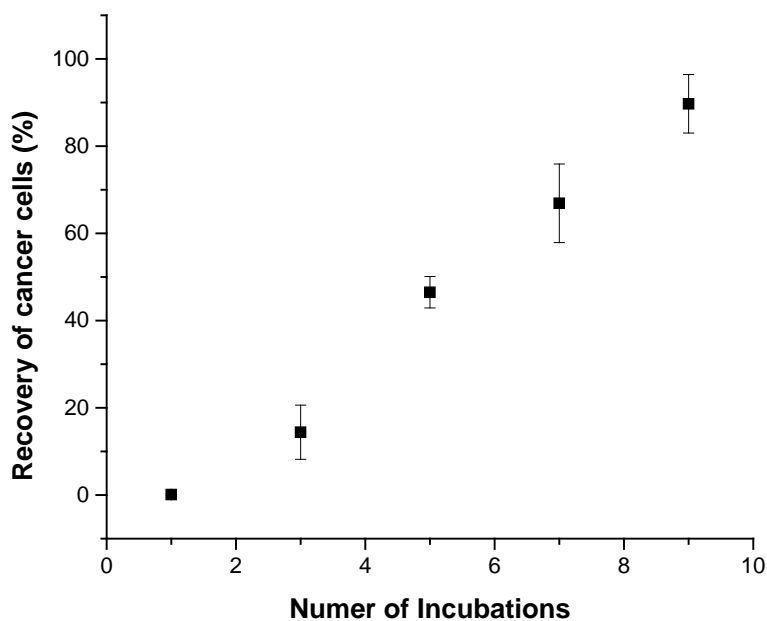


Figure 3.10. U-87 MG cells recovery after final temperature oscillation.

### 3.4. Conclusion

In summary, this research project demonstrated the ability of the patterned stimuli-responsive polymer brush to switch its properties from cell adhesive to a non adhesive surface using a mild change of temperature. The thermoresponsiveness of the polymer PNIPAM enabled the regulation of integrin-RGDS bonding. Furthermore, the switchable biointerface selective adhesiveness was successfully used to separate U87MG cells from a complex mixture of blood cells at a low U-87 MG/BC ratio to achieve a recovery of more than 90%. The method here described has the benefit of not requiring labeling and can be used without high flow rates that result in breaking the CTC clusters apart.

### 3.5. References

1. Bellis, S. L., Advantages of RGD peptides for directing cell association with biomaterials. *Biomaterials* **2011**, *32* (18), 4205-10.
2. Uhlig, K.; Boerner, H. G.; Wischerhoff, E.; Lutz, J. F.; Jaeger, M. S.; Laschewsky, A.; Duschl, C., On the Interaction of Adherent Cells with Thermoresponsive Polymer Coatings. *Polymers* **2014**, *6* (4), 1164-1177.
3. Plow, E. F.; Haas, T. A.; Zhang, L.; Loftus, J.; Smith, J. W., Ligand binding to integrins. *J Biol Chem* **2000**, *275* (29), 21785-8.
4. Humphries, J. D.; Byron, A.; Humphries, M. J., Integrin ligands at a glance. *J Cell Sci* **2006**, *119* (Pt 19), 3901-3.
5. Garcia, A. J., Get a grip: integrins in cell-biomaterial interactions. *Biomaterials* **2005**, *26* (36), 7525-9.
6. Irvine, D. J.; Mayes, A. M.; Griffith, L. G., Nanoscale clustering of RGD peptides at surfaces using comb polymers. 1. Synthesis and characterization of comb thin films. *Biomacromolecules* **2001**, *2* (1), 85-94.
7. Ho, M. H.; Wang, D. M.; Hsieh, H. J.; Liu, H. C.; Hsien, T. Y.; Lai, J. Y.; Hou, L. T., Preparation and characterization of RGD-immobilized chitosan scaffolds. *Biomaterials* **2005**, *26* (16), 3197-206.
8. Uto, K.; Tsui, J. H.; DeForest, C. A.; Kim, D. H., Dynamically Tunable Cell Culture Platforms for Tissue Engineering and Mechanobiology. *Prog Polym Sci* **2017**, *65*, 53-82.
9. Stuart, M. A.; Huck, W. T.; Genzer, J.; Muller, M.; Ober, C.; Stamm, M.; Sukhorukov, G. B.; Szleifer, I.; Tsukruk, V. V.; Urban, M.; Winnik, F.; Zauscher, S.; Luzinov, I.; Minko, S., Emerging applications of stimuli-responsive polymer materials. *Nat Mater* **2010**, *9* (2), 101-13.

10. Brittain, W. J.; Minko, S., A structural definition of polymer brushes. *J Polym Sci Pol Chem* **2007**, *45* (16), 3505-3512.
11. Cabane, E.; Zhang, X.; Langowska, K.; Palivan, C. G.; Meier, W., Stimuli-responsive polymers and their applications in nanomedicine. *Biointerphases* **2012**, *7* (1-4), 9.
12. Chen, W. L.; Cordero, R.; Tran, H.; Ober, C. K., 50th Anniversary Perspective: Polymer Brushes: Novel Surfaces for Future Materials. *Macromolecules* **2017**, *50* (11), 4089-4113.
13. Chen, T.; Ferris, R.; Zhang, J. M.; Ducker, R.; Zauscher, S., Stimulus-responsive polymer brushes on surfaces: Transduction mechanisms and applications. *Progress in Polymer Science* **2010**, *35* (1-2), 94-112.
14. Hu, J. L.; Meng, H. P.; Li, G. Q.; Ibekwe, S. I., A review of stimuli-responsive polymers for smart textile applications. *Smart Materials and Structures* **2012**, *21* (5), 53001.
15. Tugulu, S.; Silacci, P.; Stergiopoulos, N.; Klok, H. A., RGD-Functionalized polymer brushes as substrates for the integrin specific adhesion of human umbilical vein endothelial cells. *Biomaterials* **2007**, *28* (16), 2536-46.
16. Groll, J.; Fiedler, J.; Engelhard, E.; Ameringer, T.; Tugulu, S.; Klok, H. A.; Brenner, R. E.; Moeller, M., A novel star PEG-derived surface coating for specific cell adhesion. *J Biomed Mater Res A* **2005**, *74* (4), 607-17.
17. Petrie, T. A.; Raynor, J. E.; Reyes, C. D.; Burns, K. L.; Collard, D. M.; Garcia, A. J., The effect of integrin-specific bioactive coatings on tissue healing and implant osseointegration. *Biomaterials* **2008**, *29* (19), 2849-57.
18. Muszanska, A. K.; Rochford, E. T.; Gruszka, A.; Bastian, A. A.; Busscher, H. J.; Norde, W.; van der Mei, H. C.; Herrmann, A., Antiadhesive polymer brush coating functionalized with

antimicrobial and RGD peptides to reduce biofilm formation and enhance tissue integration.

*Biomacromolecules* **2014**, *15* (6), 2019-26.

19. Zhou, X. C.; Liu, X. Q.; Xie, Z.; Zheng, Z. J., 3D-patterned polymer brush surfaces.

*Nanoscale* **2011**, *3* (12), 4929-4939.

20. Huang, J.; Grater, S. V.; Corbellini, F.; Rinck, S.; Bock, E.; Kemkemer, R.; Kessler, H.;

Ding, J.; Spatz, J. P., Impact of order and disorder in RGD nanopatterns on cell adhesion. *Nano*

*Lett* **2009**, *9* (3), 1111-6.

21. Zhang, B.; Shan, H.; Li, D.; Li, Z. R.; Zhu, K. S.; Jiang, Z. B.; Huang, M. S., Different

methods of detaching adherent cells significantly affect the detection of TRAIL receptors.

*Tumori* **2012**, *98* (6), 800-803.

22. Tsai, H.-Y.; Vats, K.; Yates, M. Z.; Benoit, D. S. W., Two-Dimensional Micropatterns of

Self-Assembled Poly (N-isopropylacrylamide) Microgels for Patterned Adhesion and

Temperature-Responsive Detachment of Fibroblasts. *Langmuir: the ACS journal of surfaces and*

*colloids* **2013**, *29* (39).

23. Nash, M. E.; Healy, D.; Carroll, W. M.; Elvira, C.; Rochev, Y. A., Cell and cell sheet

recovery from pNIPAm coatings; motivation and history to present day approaches. *J Mater*

*Chem* **2012**, *22* (37), 19376-19389.

24. Cooperstein, M. A.; Canavan, H. E., Biological cell detachment from poly(N-isopropyl

acrylamide) and its applications. *Langmuir* **2010**, *26* (11), 7695-707.

25. Matsuda, T.; Saito, Y.; Shoda, K., Cell sorting technique based on thermoresponsive

differential cell adhesiveness. *Biomacromolecules* **2007**, *8* (8), 2345-9.

26. Poloukhine, A. A.; Mbua, N. E.; Wolfert, M. A.; Boons, G. J.; Popik, V. V., Selective labeling of living cells by a photo-triggered click reaction. *J. Am. Chem. Soc.* **2009**, *131* (43), 15769-76.
27. Laradji, A. M.; McNitt, C. D.; Yadavalli, N. S.; Popik, V. V.; Minko, S., Robust, Solvent-Free, Catalyst-Free Click Chemistry for the Generation of Highly Stable Densely Grafted Poly(ethylene glycol) Polymer Brushes by the Grafting To Method and Their Properties. *Macromolecules* **2016**, *49* (20), 7625-7631.
28. Khalili, A. A.; Ahmad, M. R., A Review of Cell Adhesion Studies for Biomedical and Biological Applications. *Int J Mol Sci* **2015**, *16* (8), 18149-84.
29. Lehnert, D.; Wehrle-Haller, B.; David, C.; Weiland, U.; Ballestrem, C.; Imhof, B. A.; Bastmeyer, M., Cell behaviour on micropatterned substrata: limits of extracellular matrix geometry for spreading and adhesion. *J Cell Sci* **2004**, *117* (Pt 1), 41-52.
30. Halperin, A.; Kroger, M., Thermoresponsive cell culture substrates based on PNIPAM brushes functionalized with adhesion peptides: theoretical considerations of mechanism and design. *Langmuir* **2012**, *28* (48), 16623-37.
31. Lambert, A. W.; Pattabiraman, D. R.; Weinberg, R. A., Emerging Biological Principles of Metastasis. *Cell* **2017**, *168* (4), 670-691.
32. Massague, J.; Obenauf, A. C., Metastatic colonization by circulating tumour cells. *Nature* **2016**, *529* (7586), 298-306.
33. Desgrosellier, J. S.; Cheresch, D. A., Integrins in cancer: biological implications and therapeutic opportunities. *Nat Rev Cancer* **2010**, *10* (1), 9-22.
34. Mizejewski, G. J., Role of Integrins in Cancer: Survey of Expression Patterns. *Proceedings of the Society for Experimental Biology and Medicine* **1999**, *222* (2), 124-138.

35. Cui, Y.; Song, X.; Li, S.; He, B.; Yuan, L.; Dai, W.; Zhang, H.; Wang, X.; Yang, B.; Zhang, Q., The impact of receptor recycling on the exocytosis of alphavbeta3 integrin targeted gold nanoparticles. *Oncotarget* **2017**, *8* (24), 38618-38630.
36. Nakada, M.; Nambu, E.; Furuyama, N.; Yoshida, Y.; Takino, T.; Hayashi, Y.; Sato, H.; Sai, Y.; Tsuji, T.; Miyamoto, K. I.; Hirao, A.; Hamada, J. I., Integrin alpha3 is overexpressed in glioma stem-like cells and promotes invasion. *Br J Cancer* **2013**, *108* (12), 2516-24.
37. Lagarrigue, F.; Kim, C.; Ginsberg, M. H., The Rap1-RIAM-talin axis of integrin activation and blood cell function. *Blood* **2016**, *128* (4), 479-87.

#### 4. MAGNETICALLY CONTROLLED DRUG DELIVERY SYSTEM FOR IMPLANT INFLAMMATION<sup>3</sup>

---

<sup>3</sup> Laradji, A. M.; McNitt, C. D.; Yadavalli, N. S.; Zacharchenko, A.; Popik, V. V.; Minko, S. To be submitted to angewandte chemie.

## **Abstract**

Drugs administration using the concept of targeted delivery is well recognized due to its ability to mediate a balance between the therapeutic effects and side effects of drugs. Due to concerns over the side effects, the therapeutic concentration of drugs cannot be approached which leads to only slight or no progress in treatment. In this research project, the development of an implantable drug delivery system capable of releasing its therapeutics under the influence of an external stimulus is reported. The drug delivery platform consists of a surface modified with bovine serum albumin-drug conjugate from one side and magnetic nanoparticles on which BSA-specific enzyme is immobilized from the other side. The drug release is finally induced by applying a magnetic field near the implantable device which causes the enzyme-coated magnetic nanoparticles to deposit on the surface and to immediately initiate proteolysis and drug release consequently. The implantable device was further tested against an implant inflammation by loading an anti-inflammatory drug and showed efficient control in space and time over the release of the therapeutic when the stimulus is applied.

### **4.1. Introduction**

Delivering drugs at their target site is one of the promising technologies in health care. Unlike conventional drug administration, these delivering systems offer numerous advantages such as drug concentration control, selectivity by accumulating at diseased sites, patient compliance due to reduced administration frequency, and low to no side effects.<sup>1-2</sup> The latter advantage is especially important considering that most drugs have side effects. Furthermore, any potential drug is only approved after its therapeutic benefits are shown to outweigh its risks.

Stimuli responsive materials have recently become of high interest to the scientific community due to their advantages over traditional materials in different fields of applications such as drug

delivery, diagnostics, tissue engineering, and textiles.<sup>3-4</sup> These smart materials have the capability to undergo physical or chemical changes as a response to externally applied stimuli, which makes them promising candidates to address the drawbacks often associated with the use of traditional materials, as in the case of drug delivery systems where non selectivity and inaccuracy is a major concern. Examples of commonly used stimuli to trigger a chemical or physical change within a smart responsive material include near-infrared light,<sup>5-7</sup> pH changes,<sup>8-9</sup> externally applied magnetic field,<sup>10-11</sup> and enzymes.<sup>12-14</sup>

The use of magnetic field in drug delivery to stimulate a responsive material constitutes a better approach, however, as it uses a non-invasive energy to direct the therapeutic toward the target site, and the drug release can be induced virtually anywhere in the human body. Iron oxide nanoparticles are some of the commonly used magnetic nanoparticles in drug delivery and are characterized by their improved biocompatibility, simplicity of their preparation, and affluent functional groups for further surface modification.<sup>15</sup>

One area that could possibly benefit from targeted drug delivery is the area of implantable medical devices. Implantable medical devices are used widely in various parts within the human body and have found applications in cardiovascular, orthopedics, contraception, drug delivery, pacemakers, and cosmetics.<sup>16-21</sup> These devices are exclusively implanted through surgical procedures and are meant to reside in their host organ either permanently or temporarily. Nevertheless, the introduction of a foreign device into the body is still under the burden of complications.<sup>22-25</sup> One such complication is inflammatory host response caused by biomolecules adsorption on the implant and leukocytes activation to counteract the foreign body.<sup>26</sup> These serial reaction events are known by biofouling and may incite persistent inflammatory response which could ultimately lead to implant failure.<sup>27</sup> The strategy to improve implant biocompatibility and

deter anti-inflammatory responses has been preventive by coating the implant surface with an antifouling polymer thin film such polyethylene glycol and poly (N-isopropyl acrylamide).<sup>28-30</sup> This approach, however, suffers from non-permanent aqueous stability,<sup>31</sup> in addition to conflicting outcomes concerning their capabilities in dealing with persistent inflammatory responses in-vivo.<sup>27, 32</sup> A more attractive approach for a robust and biologically stable medical implant against inflammation is to incorporate an anti-inflammatory drug that could remotely be released and locally delivered upon the application of an external and non-invasive stimulus.

Recently, we reported the development of a novel platform for the remote control of biocatalytic process and revealed its potential as a delivery system of therapeutic agents.<sup>33</sup> In that report, we demonstrated how two different kinds of polymer brush-coated magnetic nanoparticles, with one being loaded with a protease and the other with the protease-specific protein, can be merged together under the influence of an external magnetic field to liberate a protein-bound molecule. Using the same concept, we here provide a proof of concept study that describes the design and synthesis of a model medical implant with antifouling properties and capability of controlled release of a model drug to the implant immediate surroundings. The platform is composed of two different parts: the main part, which contains the model drug to be released, is made by immobilizing a protein-drug conjugate onto a silicon substrate followed by grafting a thin layer of poly(oligo(ethylene glycol) methacrylate) (POEGMA) from the surface of the silicon wafer. This thin film of POEGMA has the main objective of protecting the protein-drug conjugate from undesirable release when no trigger is applied, in addition to avoiding an immune response inside the body. The second part of the system is made of a protease that is covalently immobilized on the surface of polymer brush-coated iron oxide magnetic nanoparticles. Eventually, when an external magnetic field is applied under the drug-immobilized implant, the

two parts of the system overcome the polymer brush barriers-that prevent the interaction of different part with each other- and merge together to switch on the biocatalytic process (Figure 4.1).

As a proof of concept, we employed albumin-fluorescein isothiocyanate conjugate to monitor the proteolytic process via fluorescence spectroscopy and evaluate the antifouling properties of the model implant.

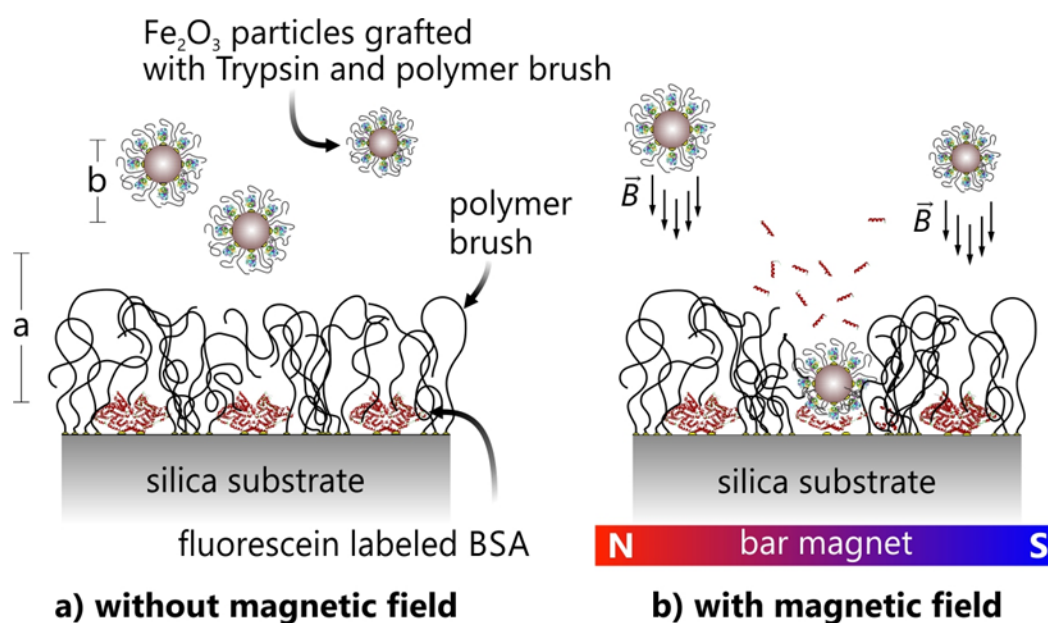


Figure 4.1. Illustration of the working concept of the stimuli responsive model implant.

## 4.2. Experimental Section

**Materials.** Silicon wafers (orientation 100, native oxide) were purchased from University Wafer (South Boston, MA). Poly(ethylene glycol) methyl ether methacrylate Mn 300 g/mol and glycidyl methacrylate were purchased from sigma and were used immediately after inhibitors removal using a basic aluminum oxide-packed column. The following reagents were similarly obtained from commercial sources and were used as received: Budesonide, 2,5-dimethoxy-4-iodoamphetamine (DOI), bovine serum albumin (BSA), albumin-fluorescein isothiocyanate

conjugate (BSA-FITC), trypsin, tetraethyl orthosilicate (TEOS), N-Hydroxysuccinimide (NHS),  $\alpha$ -Bromoisobutyryl bromide (BIBB), N-(3-Dimethylaminopropyl)-N'-ethylcarbodiimide hydrochloride (EDC), (3-Aminopropyl) triethoxysilane (APS), Copper(II) bromide, N,N,N',N'',N''-Pentamethyldiethylenetriamine (PMDETA), ascorbic acid, hydrogen peroxide, ammonium hydroxide, iron(II) chloride tetrahydrate, iron(III) chloride hexahydrate, nitric acid, sodium hydroxide, hydrochloric acid, trisodium citrate dehydrate, anhydrous dichloromethane, and chloroform. Cyclopropenone-caged dibenzocyclooctyne-amine (photo-DIBO-amine) was synthesized as previously described.<sup>42</sup>

**Measurements.** Atomic Force Microscopy (AFM) images were obtained using Bruker Multimode Nanoscope instrument in the tapping mode. A spectrometric ellipsometer from Accurion (Germany) with a fixed angle of incidence of 70° was used to measure the dry films thickness at three different locations of each sample. Ellipsometry thickness maps were generated using the Accurion software package, DataStudio. Fluorescence spectra were collected using the spectrofluorometer Fluorolog from Horiba. Nanoparticles size and zeta potential were measured by dynamic light scattering using Zetasizer Nano ZS from Malvern. Nicolet 6700 FT-IR spectrometer from Thermo Scientific was used to collect IR transmission spectra of nanoparticles. Infrared spectra of the modified silicon wafers were recorded using Nicolet model 6700 with a grazing angle attenuated total reflectance accessory at 128 scans with a resolution of 4 cm<sup>-1</sup>.

**Synthesis of the Model Implant.** Silicon wafers were first cut into square pieces of 1x1 cm<sup>2</sup> and then sonicated in chloroform, DCM, and ethanol consecutively for 5 min each before being rinsed with DI water. The silicon wafers were then soaked in a solution of 28% NH<sub>4</sub>OH/30% H<sub>2</sub>O<sub>2</sub>/DI water (1:1:1 by volume) for 1 hour at 60 °C. The substrates were rinsed with DI water

and dried under a stream of argon. Next, the substrates were placed in a 2 % solution of APS in ethanol for 6 hours at room temperature. The APS-modified silicon wafers were, next, sonicated in ethanol for 5 min and annealed for 10 min at 110°C. The next step was to introduce an ATRP initiator by reacting the primary amine functional groups of APS with BIBB. This reaction was achieved by incubating the APS-modified silicon wafers in anhydrous dichloromethane containing 2 %V/V of trimethylamine and 1 % V/V BIBB for 12 hours at room temperature. The ATRP modified substrates were then cleaned with ethanol and dried with argon. In order to covalently immobilize the protein BSA onto the surface, first, a thin layer of poly(glycidyl methacrylate) (PGMA) was generated through ARGET ATRP using the following protocol: the initiator-modified substrate was immersed in a solution containing 500 µl of DMF, 500 µl of dry acetonitrile, 9 µl Cu(II)Br (0.224 M in water), and 9 µl PMDTA (0.479 M in water). The surface initiated polymerization was started immediately upon the addition of 50 µl of ascorbic acid (0.227 M in water). After 20 min, the polymerization was stopped by exposing the reaction mixture to air and the PGMA-modified substrate was washed in ethanol and dried with argon. The protein was conjugated to the PGMA-modified substrate by reacting the protein primary amine groups with the epoxy groups of PGMA.<sup>43</sup> 5 mg/ml in PBS buffer of either BSA or BSA-FITC was added to the substrate and reacted for 12 hours at RT. The substrates were washed with PBS buffer, SDS (0.1 M in water) for 30 minutes, and water to wash away the loosely adsorbed protein molecules. A final thin layer of poly oligo(ethylene glycol) methyl ether methacrylate (POEGMA) was generated from the end-group bromine of PGMA by adopting the same aforementioned surface-initiated polymerization protocol and using Poly(ethylene glycol) methyl ether methacrylate (500 µl) as the monomer and ethanol/water (500 µl/500 µl) as the solvent. In the case of BSA, another step was undertaken which consisted of conjugating either

Budesonide, or 2,5-dimethoxy-4-iodoamphetamine to BSA. This step was completed by first activating the carboxylic groups of BSA-modified substrate with EDC (20 mg/ml in MES buffer pH 5.5) and NHS (25 mg/ml in MES buffer pH 5.5) for 1 hour at room temperature, followed by reacting the anti-inflammatory drugs (1 mg/ml in water/DMF) with the activated BSA at room temperature overnight. The substrates were finally washed with water and dried with argon.

**Synthesis of Trypsin-Coated Iron Oxide Magnetic Nanoparticles (MNPs-TRY).** Iron oxide magnetic nanoparticles were synthesized and coated with a silica shell using a previously reported approach.<sup>33, 44</sup> The magnetite-silica core-shell nanoparticles were next modified with a PGMA-POEGMA copolymer to create anchoring groups for the enzyme trypsin and confer a good stability of the nanoparticles in aqueous media. First, the nanoparticles were stirred overnight in a solution of dry toluene/acetonitrile (V/V: 1/3) containing 1 % (3-Glycidyloxypropyl)trimethoxysilane, and then centrifuged and washed thrice with acetonitrile. The GPS-modified nanoparticles were ultimately redispersed in DMF/acetonitrile V/V: 1/1. The epoxy groups of GPS were, next, used to attach photo-DIBO for 24 hour, which was deprotected afterward using a UV light and reacted with a synthesized azide-terminated PGMA following our previously reported protocol.<sup>45</sup> The copolymerization of Poly(ethylene glycol) methyl ether methacrylate from bromine-terminated PGMA was then completed according to a previous report,<sup>33</sup> followed by the immobilization of trypsin (10 mg/ml in PBS buffer pH 7.4) for 12 hours at room temperature. Finally, the trypsin-immobilized nanoparticles were centrifuged and washed with sodium acetate solution (20 mM, pH 3.2) to desorb the loosely attached trypsin molecules.<sup>46</sup>

**Protein Digestion and Trigger Release Experiments.** The Model drug-modified implant was immersed in PBS buffer containing MNPs-TRY and the temperature was adjusted to 37 °C. In

order to initiate the biocatalytic reaction, an external magnetic field was positioned near the implant, and the digestion progress was monitored by fluorescence spectroscopy ( $\lambda_{ex} = 485$  nm,  $\lambda_{em} = 505-650$  nm for BSA-FiTC). To assess the antifouling properties of the model implant, the BSA-FiTC-modified substrates with different thicknesses of POEGMA were immersed in solutions of PBS buffer containing 100 mM trypsin. Trypsin molecules ability to reach BSA-FiTC was monitored with fluorescence spectroscopy.

### 4.3. Results and Discussion

**Synthesis of the Model Implant.** The model implant is designed to contain a BSA-drug conjugate immobilized on the surface and imbedded into a thin polymer layer that serves as a shield between the implant and biomolecules in the immediate environment. A PGMA layer was first created from the surface of silicon wafers using surface-initiated ARGET ATRP. The use of PGMA as an anchoring layer for subsequent modifications by synthetic and natural polymers has previously been employed.<sup>34</sup> The epoxy groups of PGMA are reactive toward many nucleophiles through an epoxy ring opening reaction and this reactivity increases in aqueous media.<sup>35</sup> Furthermore, PGMA provides more stability in aqueous media due to its hydrophobic nature and the self-healing properties.<sup>36-37</sup> The surface-initiated polymerization of GMA was done for 20 min to yield a PGMA film of ~ 15 nm thicknesses (Figure 4.2b). Immobilization of BSA on PGMA was done in PBS buffer and the successful reaction was confirmed with grazing-angle FTIR. POEGMA thin layer was generated using surface-initiated ARGET ATRP from bromine-terminated PGMA. Ellipsometry, AFM and grazing-angle FTIR were used to characterize the final product. During this step, POEGMA layers of various thicknesses were generated to investigate the dependence of the antifouling properties of the model implant on POEGMA thickness. The FTIR spectra shown in figure 4.2a reveal the successful immobilization of

PGMA. The appearance of the peaks at  $1731\text{ cm}^{-1}$  and  $1143\text{ cm}^{-1}$  are characteristics of the carbonyl and ether stretch vibrations consecutively. Furthermore, the  $\text{sp}^3$  stretch peaks of C-H are apparent at  $2900\text{ cm}^{-1}$ . After BSA immobilization on PGMA, new peaks appeared at  $1652\text{ cm}^{-1}$  and  $1534\text{ cm}^{-1}$  from amide I and amide II, indicating the successful opening of epoxy moieties by BSA lysine groups. FTIR spectra also reveal the successful generation of POEGMA through a strong peak at  $1103\text{ cm}^{-1}$  of C-O bond stretch. The thickness of POEGMA was estimated by ellipsometry, and the step-by-step thickness map reveals the macroscopic uniformity of each layer at a large scale. At a microscopic scale, AFM microscopy (Figure 4.3) shows the complete coverage and smooth nature of all layers.

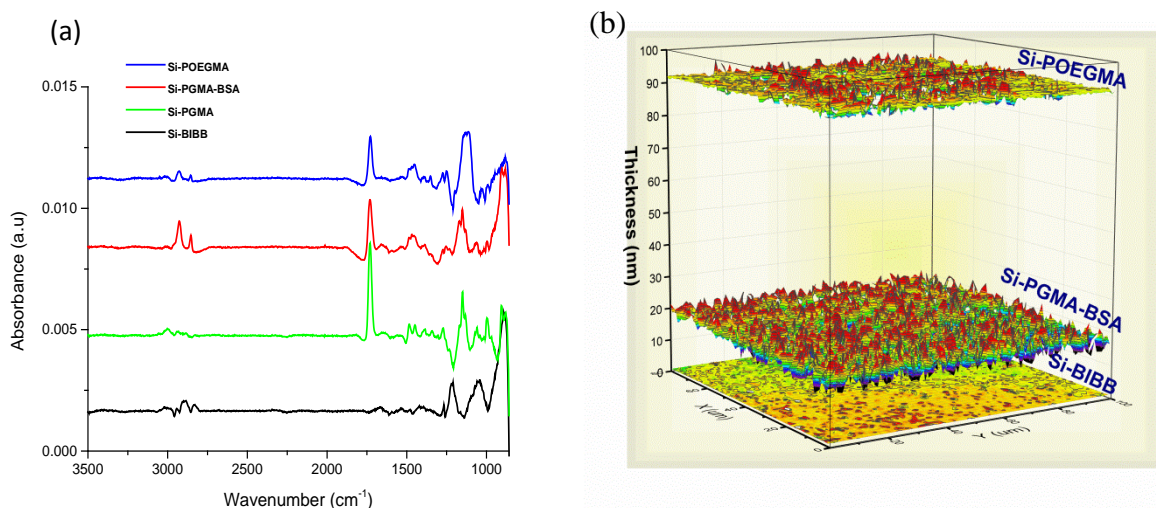


Figure 4.2. FTIR grazing angle (a) and ellipsometry maps (b) of the substrate layers.

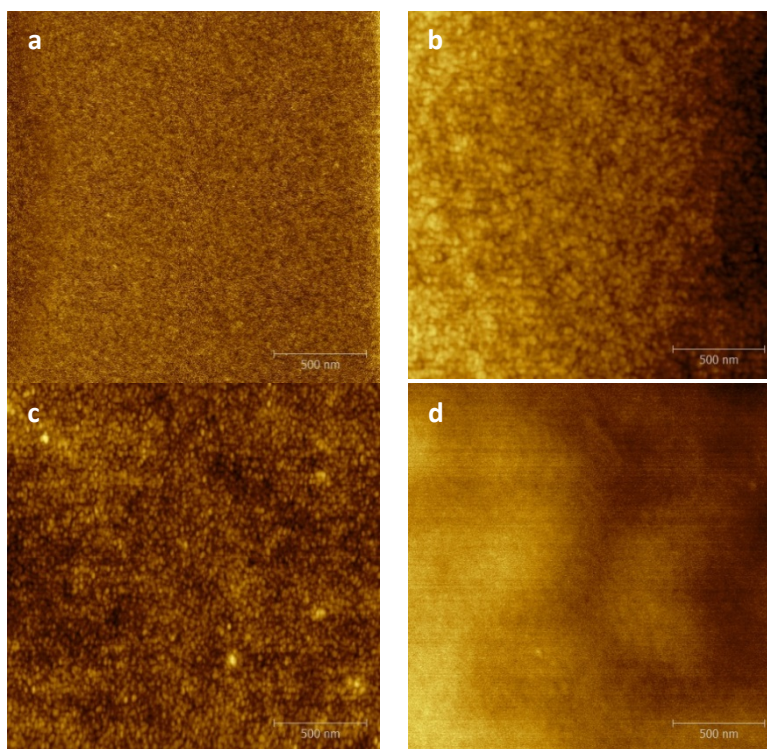


Figure 4.3. AFM height images of Si-BIBB (a), Si-PGMA (b), Si-BSA (c), and Si-POEGMA (d).

**Synthesis of Trypsin-Coated Iron Oxide Magnetic Nanoparticles.** The enzyme-conjugated magnetic nanoparticles (MNPs-TRY) were here designed by taking into account possible undesired interactions between trypsin and its environment. In our previous report,<sup>33</sup> we have shown that enzyme chemical structure and its activity are not compromised by enzyme conjugation. This was further confirmed by carrying out enzyme activity test using ENZCHECK (figure 4.4b). Furthermore, protein-conjugated magnetic nanoparticles do not interact with each other when the magnetic field is turned off due to the shielding effect exerted by a POEGMA thin layer enveloping the enzyme molecules. The amount of enzyme conjugated onto the magnetic nanoparticles was estimated by subtracting the measured UV absorption of the supernatant at 280 nm from that of trypsin solution prior to the reaction. Using a calibration curve of standard

protein solutions, the immobilized trypsin was estimated to be 82.96  $\mu\text{g}/\text{mg}$  of copolymer-grafted nanoparticles (or 41.96  $\mu\text{g}/\text{ml}$ ). Moreover, FTIR spectra after each step were recorded. As shown in figure 4.4a, the absorption at 1064  $\text{cm}^{-1}$  is characteristic of the Si-O-Si vibration mode. Upon reacting azide-terminated PGMA with DIBO-immobilized nanoparticles, a peak at 1724  $\text{cm}^{-1}$  appears that represents the carbonyl stretch. The reaction success was furthermore confirmed with the disappearance of azide peak at around 2200  $\text{cm}^{-1}$  (data not shown). Finally, trypsin immobilization on the POEGMA-PGMA-modified magnetic nanoparticles was apparent from the appearance of amide peaks at 1647  $\text{cm}^{-1}$  and 1532  $\text{cm}^{-1}$  from amide I and amide II. The nanoparticles sizes were measured with DLS and are presented by figure 4.4c. Initially, the iron oxide magnetic nanoparticles had an average diameter of 15-20 nm that changed to 40 nm upon silica coating of nanoparticles. The nanoparticles size changed again from ~40 nm to ~50-60 nm and then to ~90-110 nm upon PGMA and POEGMA immobilization consecutively. It's noteworthy to mention that the magnetic nanoparticles became very stable colloidal dispersion in aqueous media upon adding POEGMA. Furthermore, the POEGMA outer layer is anticipated to confer the nanoparticles low degradation and increased blood circulation time, in addition to low cytotoxicity,<sup>38-39</sup> which are important requirements for the nanoparticles to reach their target and trigger the drug release.

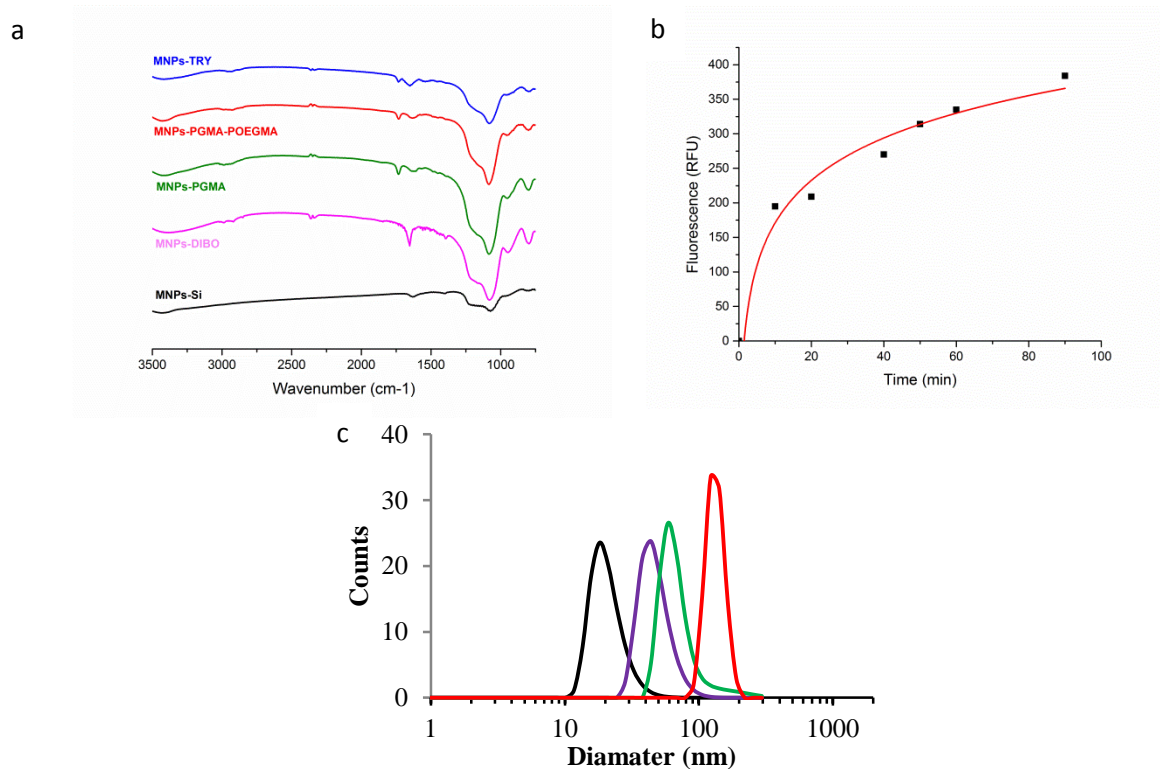


Figure 4.4. FTIR spectra (a), enzyme activity of MNPs-TRY(b), and particle size by DLS of MNPs (black), MNPs-Si (purple), MNPs-PGMA (green), and MNPs-POEGMA (red) (c)

**Protein Digestion and Trigger Release Experiments.** To determine the optimum thickness of POEGMA necessary to deter undesired interactions of the model implant with surrounding biomolecules, BSA-FITC-immobilized substrates were modified with different thicknesses of POEGMA and then immersed in solutions of PBS buffer containing 100 mM trypsin. Figure 4.5 shows the effects POEGMA thickness on BSA proteolysis where it is clearly seen that higher POEGMA thicknesses (at least 70 nm) totally prevent trypsin from reaching BSA. Proteolysis was evident in absence of any POEGMA layer while it was also observed at 20 and 50 nm but at a lesser extent.

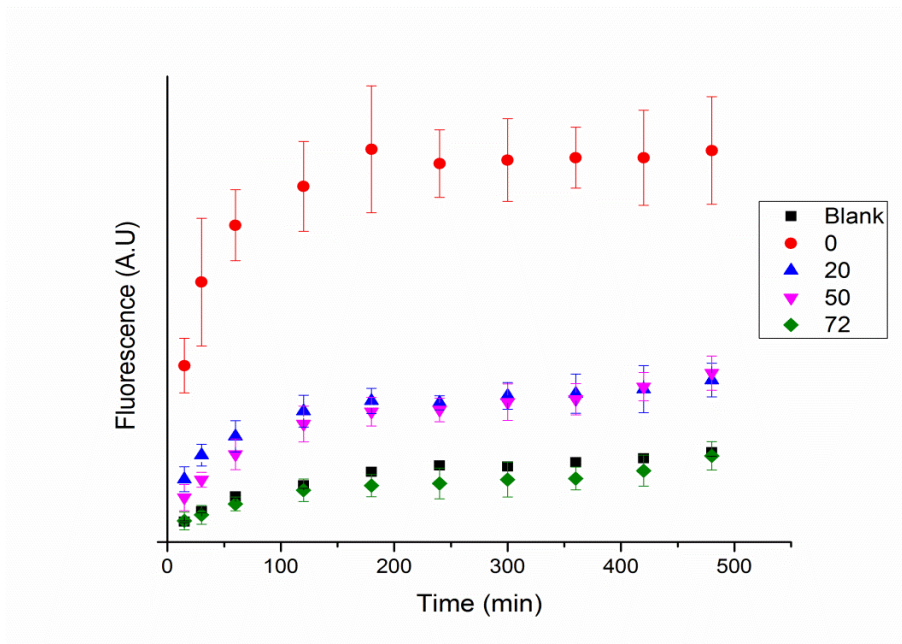


Figure 4.5. Thickness of POEGMA effects on proteolysis.

For BSA-FiTC proteolysis using trypsin-immobilized magnetic nanoparticles, the process was monitored under and without the influence of an external magnetic field using fluorescence spectroscopy. Figure 4.6a reports the kinetics of FiTC-peptides release from the substrate as a result of BSA-FiTC proteolysis. Under the influence of an external magnetic field, trypsin-coated MNPs were brought into contact with the model implant almost immediately causing the BSA digestion and FiTC-peptides release to initiate promptly. This led to a rapid BSA-FiTC digestion where most of the FiTC release was observed to occur within one hour. After that, BSA-FiTC proteolysis continued though at a slower rate. The maximum FiTC fluorescence intensity was reached after about 6 hours of reaction, since the fluorescence signal didn't change significantly afterwards. The efficiency of the process was estimated to be about 55 % by ascribing 100 % to the proteolysis process of BSA-FiTC in trypsin solution (100 mM). During the same period of 6 hours, BSA-FiTC digestion in the absence of any magnetic field was significantly less (Figure 4.6b) as trypsin modified magnetic nanoparticles were well dispersed

and undisturbed in the digestion buffer. Moreover, the shielding effect provided by the thin layer of PEOGMA brush may have prevented gravity-induced deposited nanoparticles from reaching BSA-FITC.

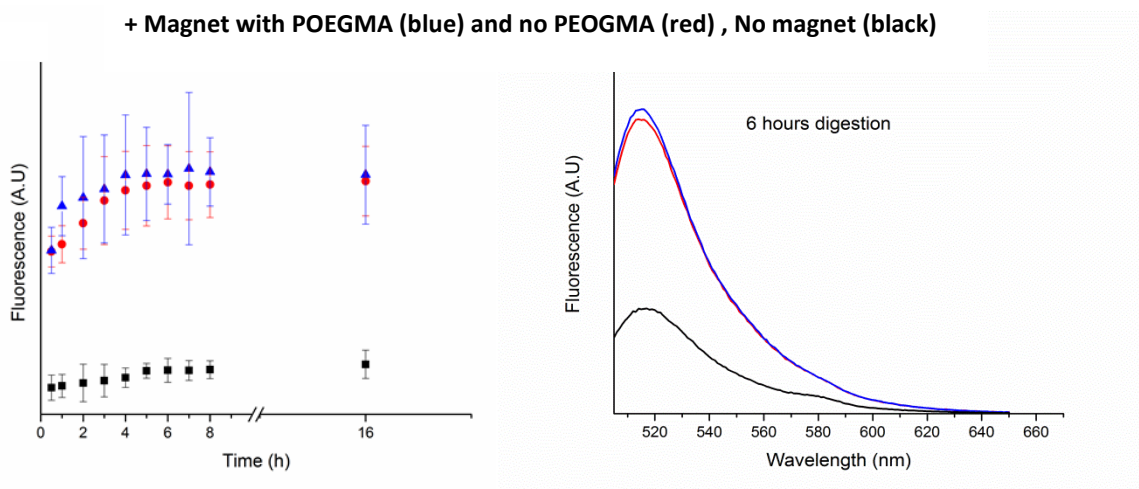


Figure 4.6. BSA-FITC proteolysis under and without the influence of a magnetic field.

#### 4.4. Conclusion

In summary, a stimuli-responsive drug release from a model implant has been demonstrated using a remotely controlled biocatalytic process. The drug release is stimulated by the application of an external magnetic field that causes enzyme-modified magnetic nanoparticles to accumulate on a drug-protein conjugate immobilized on substrate and initiate the protein digestion. The model implant was loaded with actual anti-inflammatory drugs and exhibited selective drug release and cytokine inhibition only when the external stimulus is applied. The drug delivery platform here reported could potentially find further applications in fields where controlling the special and temporal delivery of chemical and biological entities is desired.

#### 4.5. References

1. Malachowski, K.; Breger, J.; Kwag, H. R.; Wang, M. O.; Fisher, J. P.; Selaru, F. M.; Gracias, D. H., Stimuli-Responsive Theragrippers for Chemomechanical Controlled Release. *Angewandte Chemie* **2014**, *126* (31), 8183-8187.

2. Srinivasarao, M.; Low, P. S., Ligand-Targeted Drug Delivery. *Chem Rev* **2017**, *117* (19), 12133-12164.
3. Stuart, M. A.; Huck, W. T.; Genzer, J.; Muller, M.; Ober, C.; Stamm, M.; Sukhorukov, G. B.; Szleifer, I.; Tsukruk, V. V.; Urban, M.; Winnik, F.; Zauscher, S.; Luzinov, I.; Minko, S., Emerging applications of stimuli-responsive polymer materials. *Nat Mater* **2010**, *9* (2), 101-13.
4. Wang, Y.; Shim, M. S.; Levinson, N. S.; Sung, H. W.; Xia, Y., Stimuli-Responsive Materials for Controlled Release of Theranostic Agents. *Adv Funct Mater* **2014**, *24* (27), 4206-4220.
5. Ju, E.; Li, Z.; Liu, Z.; Ren, J.; Qu, X., Near-infrared light-triggered drug-delivery vehicle for mitochondria-targeted chemo-photothermal therapy. *ACS Appl Mater Interfaces* **2014**, *6* (6), 4364-70.
6. Kurapati, R.; Raichur, A. M., Near-infrared light-responsive graphene oxide composite multilayer capsules: a novel route for remote controlled drug delivery. *Chem Commun (Camb)* **2013**, *49* (7), 734-6.
7. Yang, X.; Liu, X.; Liu, Z.; Pu, F.; Ren, J.; Qu, X., Near-infrared light-triggered, targeted drug delivery to cancer cells by aptamer gated nanovehicles. *Adv Mater* **2012**, *24* (21), 2890-5.
8. Song, L.; Ho, V. H.; Chen, C.; Yang, Z.; Liu, D.; Chen, R.; Zhou, D., Efficient, pH-triggered drug delivery using a pH-responsive DNA-conjugated gold nanoparticle. *Adv Healthc Mater* **2013**, *2* (2), 275-80.
9. Tan, L.; Yang, M. Y.; Wu, H. X.; Tang, Z. W.; Xiao, J. Y.; Liu, C. J.; Zhuo, R. X., Glucose- and pH-responsive nanogated ensemble based on polymeric network capped mesoporous silica. *ACS Appl Mater Interfaces* **2015**, *7* (11), 6310-6.

10. Hu, B.; Du, H. J.; Yan, G. P.; Zhuo, R. X.; Wu, Y.; Fan, C. L., Magnetic polycarbonate microspheres for tumor-targeted delivery of tumor necrosis factor. *Drug Deliv* **2014**, *21* (3), 204-212.
11. Qin, J.; Asempah, I.; Laurent, S.; Fornara, A.; Muller, R. N.; Muhammed, M., Injectable Superparamagnetic Ferrogels for Controlled Release of Hydrophobic Drugs. *Advanced Materials* **2009**, *21* (13), 1354-1357.
12. He, H.; Sun, L.; Ye, J.; Liu, E.; Chen, S.; Liang, Q.; Shin, M. C.; Yang, V. C., Enzyme-triggered, cell penetrating peptide-mediated delivery of anti-tumor agents. *J Control Release* **2016**, *240*, 67-76.
13. Ding, Y.; Kang, Y.; Zhang, X., Enzyme-responsive polymer assemblies constructed through covalent synthesis and supramolecular strategy. *Chem Commun (Camb)* **2015**, *51* (6), 996-1003.
14. Giri, S.; Trewyn, B. G.; Stellmaker, M. P.; Lin, V. S., Stimuli-responsive controlled-release delivery system based on mesoporous silica nanorods capped with magnetic nanoparticles. *Angew Chem Int Ed Engl* **2005**, *44* (32), 5038-44.
15. Huang, J.; Li, Y.; Orza, A.; Lu, Q.; Guo, P.; Wang, L.; Yang, L.; Mao, H., Magnetic Nanoparticle Facilitated Drug Delivery for Cancer Therapy with Targeted and Image-Guided Approaches. *Adv Funct Mater* **2016**, *26* (22), 3818-3836.
16. Joung, Y. H., Development of implantable medical devices: from an engineering perspective. *Int Neurorol J* **2013**, *17* (3), 98-106.
17. Elango, K.; Curtis, A. B., Cardiac implantable electrical devices in women. *Clin Cardiol* **2018**.

18. Suhardi, V. J.; Bichara, D. A.; Kwok, S.; Freiberg, A. A.; Rubash, H.; Malchau, H.; Yun, S. H.; Muratoglu, O. K.; Oral, E., A Fully Functional Drug-Eluting Joint Implant. *Nat Biomed Eng* **2017**, *1*.
19. Chen, M. J.; Hsia, J. K.; Creinin, M. D., Etonogestrel implant use in women primarily choosing a combined oral contraceptive pill: A proof-of-concept trial. *Contraception* **2018**.
20. Li, J.; Liu, X.; Crook, J. M.; Wallace, G. G., Development of a porous 3D graphene-PDMS scaffold for improved osseointegration. *Colloids Surf B Biointerfaces* **2017**, *159*, 386-393.
21. Webber, M. J.; Langer, R., Drug delivery by supramolecular design. *Chem Soc Rev* **2017**, *46* (21), 6600-6620.
22. Wellman, S. M.; Kozai, T. D. Y., Understanding the Inflammatory Tissue Reaction to Brain Implants To Improve Neurochemical Sensing Performance. *ACS Chem Neurosci* **2017**, *8* (12), 2578-2582.
23. Thomas, P., Clinical and diagnostic challenges of metal implant allergy using the example of orthopaedic surgical implants: Part 15 of the Series Molecular Allergology. *Allergo J Int* **2014**, *23* (6), 179-185.
24. Beech, I. B.; Sunner, J. A.; Arciola, C. R.; Cristiani, P., Microbially-influenced corrosion: damage to prostheses, delight for bacteria. *Int J Artif Organs* **2006**, *29* (4), 443-52.
25. Gorbet, M. B.; Sefton, M. V., Biomaterial-associated thrombosis: roles of coagulation factors, complement, platelets and leukocytes. *Biomaterials* **2004**, *25* (26), 5681-703.
26. Xu, L. C.; Siedlecki, C. A., Effects of surface wettability and contact time on protein adhesion to biomaterial surfaces. *Biomaterials* **2007**, *28* (22), 3273-83.

27. Bridges, A. W.; Garcia, A. J., Anti-inflammatory polymeric coatings for implantable biomaterials and devices. *J Diabetes Sci Technol* **2008**, *2* (6), 984-94.
28. Unsworth, L. D.; Sheardown, H.; Brash, J. L., Protein-resistant poly(ethylene oxide)-grafted surfaces: chain density-dependent multiple mechanisms of action. *Langmuir* **2008**, *24* (5), 1924-9.
29. Unsworth, L. D.; Sheardown, H.; Brash, J. L., Polyethylene oxide surfaces of variable chain density by chemisorption of PEO-thiol on gold: adsorption of proteins from plasma studied by radiolabelling and immunoblotting. *Biomaterials* **2005**, *26* (30), 5927-33.
30. Singh, N.; Bridges, A. W.; García, A. J. J.; Lyon, L. A., Covalent tethering of functional microgel films onto poly(ethylene terephthalate) surfaces. *Biomacromolecules* **2007**, *8* (10), 3271-3275.
31. Paripovic, D.; Klok, H.-A., Improving the Stability in Aqueous Media of Polymer Brushes Grafted from Silicon Oxide Substrates by Surface-Initiated Atom Transfer Radical Polymerization. *Macromolecular Chemistry and Physics* **2011**, *212* (9), 950-958.
32. Shen, M.; Martinson, L.; Wagner, M. S.; Castner, D. G.; Ratner, B. D.; Horbett, T. A., PEO-like plasma polymerized tetraglyme surface interactions with leukocytes and proteins: in vitro and in vivo studies. *J Biomater Sci Polym Ed* **2002**, *13* (4), 367-90.
33. Zakharchenko, A.; Guz, N.; Laradji, A. M.; Katz, E.; Minko, S., Magnetic field remotely controlled selective biocatalysis. *Nature Catalysis* **2017**, *1* (1), 73-81.
34. Zdyrko, B.; Varshney, S. K.; Luzinov, I., Effect of molecular weight on synthesis and surface morphology of high-density poly(ethylene glycol) grafted layers. *Langmuir* **2004**, *20* (16), 6727-35.

35. Azizi, N.; Saidi, M. R., Highly chemoselective addition of amines to epoxides in water. *Org Lett* **2005**, *7* (17), 3649-51.
36. Divandari, M.; Dehghani, E. S.; Spencer, N. D.; Ramakrishna, S. N.; Benetti, E. M., Understanding the effect of hydrophobic protecting blocks on the stability and biopassivity of polymer brushes in aqueous environments: A Tiramisù for cell-culture applications. *Polymer* **2016**, *98*, 470-480.
37. Kuroki, H.; Tokarev, I.; Nykypanchuk, D.; Zhulina, E.; Minko, S., Stimuli-Responsive Materials with Self-Healing Antifouling Surface via 3D Polymer Grafting. *Advanced Functional Materials* **2013**, *23* (36), 4593-4600.
38. Ulbrich, K.; Hola, K.; Subr, V.; Bakandritsos, A.; Tucek, J.; Zboril, R., Targeted Drug Delivery with Polymers and Magnetic Nanoparticles: Covalent and Noncovalent Approaches, Release Control, and Clinical Studies. *Chem Rev* **2016**, *116* (9), 5338-431.
39. Jain, T. K.; Reddy, M. K.; Morales, M. A.; Leslie-Pelecky, D. L.; Labhasetwar, V., Biodistribution, clearance, and biocompatibility of iron oxide magnetic nanoparticles in rats. *Mol Pharm* **2008**, *5* (2), 316-27.
40. Finkin-Groner, E.; Moradov, D.; Shifrin, H.; Bejar, C.; Nudelman, A.; Weinstock, M., Indoline-3-propionate and 3-aminopropyl carbamates reduce lung injury and pro-inflammatory cytokines induced in mice by LPS. *Br J Pharmacol* **2015**, *172* (4), 1101-13.
41. Yu, B.; Becnel, J.; Zerfaoui, M.; Rohatgi, R.; Boulares, A. H.; Nichols, C. D., Serotonin 5-hydroxytryptamine(2A) receptor activation suppresses tumor necrosis factor-alpha-induced inflammation with extraordinary potency. *J Pharmacol Exp Ther* **2008**, *327* (2), 316-23.

42. Poloukhine, A. A.; Mbua, N. E.; Wolfert, M. A.; Boons, G. J.; Popik, V. V., Selective labeling of living cells by a photo-triggered click reaction. *J Am Chem Soc* **2009**, *131* (43), 15769-76.
43. Yadavalli, N. S.; Borodinov, N.; Choudhury, C. K.; Quiñones-Ruiz, T.; Laradji, A. M.; Tu, S.; Lednev, I. K.; Kuksenok, O.; Luzinov, I.; Minko, S., Thermal Stabilization of Enzymes with Molecular Brushes. *ACS Catalysis* **2017**, *7* (12), 8675-8684.
44. Deng, Y.-H.; Wang, C.-C.; Hu, J.-H.; Yang, W.-L.; Fu, S.-K., Investigation of formation of silica-coated magnetite nanoparticles via sol-gel approach. *Colloids and Surfaces A: Physicochemical and Engineering Aspects* **2005**, *262* (1-3), 87-93.
45. Laradji, A. M.; McNitt, C. D.; Yadavalli, N. S.; Popik, V. V.; Minko, S., Robust, Solvent-Free, Catalyst-Free Click Chemistry for the Generation of Highly Stable Densely Grafted Poly(ethylene glycol) Polymer Brushes by the Grafting To Method and Their Properties. *Macromolecules* **2016**, *49* (20), 7625-7631.
46. Kao, K. C.; Lin, T. S.; Mou, C. Y., Enhanced Activity and Stability of Lysozyme by Immobilization in the Matching Nanochannels of Mesoporous Silica Nanoparticles. *J Phys Chem C* **2014**, *118* (13), 6734-6743.

## 5. SUMMARY AND FUTURE OUTLOOK

### 5.1. Summary

The design and development of three different biomaterials for cells antifouling, targeted drug delivery, and cells adhesion control was here reported. First, densely grafted polymer brushes of poly(ethylene glycol) were achieved using solvent-free, catalyst-free click chemistry by the grafting to approach. The method developed yielded high grafting densities and brush thicknesses. Furthermore, the obtained PEG brushes exhibited high antifouling properties and longer stability in aqueous media.

Second, a stimuli-responsive biomaterial was developed to induce cells adhesion and detachment via the regulation of cells integrin-RGD bond using a mild change of temperature. As a practical application, the switchable interface was successfully used to isolate a small number of cancer cells from a mixture of blood cells using temperature oscillation during the process.

Finally, a novel dual stimuli responsive platform via the controlled digestion of bovine serum albumin with trypsin-loaded iron oxide magnetic nanoparticles was developed. The drug release was simply achieved by subjecting the responsive platform to an external magnetic field causing BSA proteolysis by trypsin and initiating the drug release immediately.

### 5.2. Future Work

The successful development of the biomaterials here discussed constitutes starting points for long-term research projects. The following points are some examples of a logical extension of this work:

The developed targeted drug delivery interface could be investigated for cancer drugs delivery as an implantable delivery device considering that cytotoxic drugs have harsh side effects.

Furthermore combining this approach with an active drug delivery method such as RGD labeling on the magnetic nanoparticles could enhance the drug selectivity.

We have shown that cancer cells could be efficiently detected and isolated from a complex mixture of cells using a patterned switchable biointerface. This biointerface could potentially be investigated as a cheap and convenient means to study the behavior and responsiveness of abnormal cells upon presenting and hiding biomolecules to the cells surface.

Finally, incorporating other cells recognition motifs that are selective to the abnormal cells should enable the isolation of more than one kind of cells considering that integrin is not overexpressed by all malignant cells.